Title
Can a Self-Expanding Pediatric Stent Grow with an Artery? Relationship of Stent Design to Vascular Biology

Author
Nia, Nima Vahdati

Publication Date
2020

Peer reviewed|Thesis/dissertation

UNIVERSITY OF CALIFORNIA

Los Angeles

Can a Self-Expanding Pediatric Stent Grow with an Artery? Relationship of Stent Design to Vascular Biology

A dissertation submitted in partial satisfaction of the

requirements for the degree Doctor of Philosophy

in Bioengineering

by

Nima Vahdati Nia

2020

ABSTRACT OF THE DISSERTATION

Can a self-Expanding Pediatric Stent Grow with an Artery? Relationship of Stent Design to Vascular Biology

by

Nima Vahdati Nia

Doctor of Philosophy in Bioengineering

University of California, Los Angeles, 2020

Professor Daniel Steven Levi, Co-Chair

Professor Kalyanam Shivkumar, Co-Chair

Background:

Unlike adults, children quickly outgrow any intravascular metal stents. Great interest exists in the development of stents that can either grow with or resorb in the arteries. This study aimed to develop self-expanding stents that could grow with the vasculature, examine them in a chronic animal model of a growing swine, and investigate the effects of the stent's geometry and radial forces on the growing tissue.

Methods:

Computer Aided Design (CAD) and Finite Element Analysis (FEA) was used to select four self-expanding nitinol stents with a range of radial forces. Stents were designed and manufactured to meet predetermined mechanical specifications including crossing profile and fully expanded stent size of ≥20 mm. Hysteresis plots were determined for each stent. Fourteen stents were implanted in the abdominal aorta and iliac artery of four three-months old, 50 kg swine. Quantitative angiography, and both gross pathology and histopathology was assessed at 3 months (n=2) and 6 months (n=12).

Results:

The luminal area of all stented vessels grew more than the adjacent non-stented vessels and the average rate of diameter growth was 34%–49% and 20%–23% for stented and non-stented vessels, respectively. There was no intraluminal thrombus or significant stenosis seen in any of the arteries. Variable degrees of compression and laceration of the internal elastic lamina and/or media was observed to correlate with the initial vessel size but not with the radial force of the stent on the vessel. Similar correlation was observed with inflammatory response and with the degree of neointimal formation. No animals had major complications, issues with deployment, dissection, aneurysm formation, stent fracture, or migration during vessel growth.

Conclusions:

Self-expanding stents can be designed to grow with an artery to mirror and even exceed somatic growth. Although longer term testing is needed, it is possible to make custom tailor self-expanding stents to grow after arterial implantation in pediatric patients.

The dissertation of Nima Vahdati Nia is approved.

Xiaochun, Li

Gregory P. Carman

Kalyanam Shivkumar, Co-Chair

Daniel Steven Levi, Co-Chair

University of California, Los Angeles

2020

Dedicated to my parents who are the pillars of my success, my family, and my advisor Dr. Levi for their support.

TABLE OF CONTENTS

LIST OF FIGURES

LIST OF TABLES

ACKNOWLEDGEMENTS

I would like to express my sincere appreciation to Professor Daniel S. Levi for his support and guidance through this research. Without his guidance and constant support this project was not possible. I would also like to thank Professor Li, Professor Carman, and Professor Shivkumar for their valuable suggestions and helpful insights, and spending their precious time serving in my committee. I also greatly appreciate the support and encouragement of Mark Dehdashtian whose initial support made this journey possible. In addition, I would like to thank Ali Mirnajafi for his encouragement for me to pursuit my PhD, and Edwards Lifesciences for the generous support of this research. Finally, without support of Stan Rowe and Todd Brinton this achievement was not possible.

VITA

Education

M. S., Applied Science and Technology **2016**

University of California, Berkeley

M. S., Biomedical Engineering, **2009**

University of California, Irvine

B. S., Biomedical Engineering, Specialty in Biophotonics **2008**

Cum Laude Honor Graduate

University of California, Irvine

Work Experience

Sr. Manager Engineering R&D– Clinical Usability Center of Excellence **2017-Present**

Edwards Lifesciences, Irvine Ca

Subject matter expert in the Clinical Usability Center of Excellence, managing clinical engineering group. Responsible in developing a state-of-the-art realistic mechanical pulsatile bench top tester utilizing patient's anatomy 3D print parts, human cadaver hearts and/or animal isolated hearts for physician training, R&D, and device procedural developments.

R&D Engineer – Transcatheter Heart Valves **2008-2017**

Edwards Lifesciences, Irvine Ca

Key member of the design and technical team of SAPIEN, SAPIEN XT, SAPIEN 3, and CENTERA, Transcatheter Heart Valves (THV), OPUS device for Heart Failure with Reduce Ejection Fraction (HFREF). Project leader and manager for all the design verification and validation testing that was required by ISO-5840 and FDA Heart valve guidance for Edwards Transcatheter Heart valves.

Publications

Russell, MR, Blais, B, **Nia, N**, Levi, DS. The potential impact and timeline of engineering on congenital interventions. *Pediatr. Cardiol.* 2020; 41:522-538.

Presentation

Levi, DS, **Nia, VN**. Self-expanding Nitinol growth stent for neonatal coarctation. *Pediatric and Adult Interventional Cardiac Symposium*. 2020

Patents

Keidar Y, **Nia VN**, Rowe SJ, Cao H, Reich T, cinching of dilated heart muscle 2018, US20190151093

Submitted and pending publication

Nia VN, Su B, Cao H, Tripathy S, Dominick D, Hybrid pulmonary valve anchor 2018, Application ID#: 62/769117 Patent ID#: 81095895

Nia VN, Gordon IP, Cao H, Novel anchor approach to fix HFREF through Transeptal percutaneous procedure2018, Application ID#: 62/757299 Patent ID#: 81096741

Nia VN, Cao H, Anchor for heart failure 2019, Application ID#: 62/805065 Patent ID#: 81097897

Nia VN, Dominick DT, Su B, Cao H, Tripathy S. Double valve mitral and Tricuspid replacement 2018, Application ID#: 62/811453, Patent ID#: 81098286

Sugijoto AT, **Nia VN,** Su B, Dominick DT, Cao H, Tripathy S. Papillary Muscle location restoration device for MR improvement 2019, Application ID# 62/926258 Patent ID #: 81103663

Su B, **Nia VN,** Dominick DT, Cao H, Tripathy S. Transcatheter mitral and tricuspid stiffeners 2018, Application ID# 62/890530, Patent ID#: 81101585.

CHAPTER 1: INTRODUCTION

Because exponential growth limits the use of current metallic stents in rapidly growing children, there is a great interest among the pediatric research community for stents that can either grow with an artery or be resorbed[1]. Bioresorbable stents have issues related to the effects of their degradation products on the biology of the vessel.[1,2] Current stents in the market usually require redilation to compensate for somatic growth and to avoid stenosis. We sought to design several self-expanding stents with low crimp profile of <6 Fr and large expanded diameter of 20mm. The designed stents have single row design, with large amplitude, struts with smooth corners and a range of outward radial forces that we predicted to have the ability to adapt their geometries to the potentially large increase in the aortic dimensions over time. This device's effect on rapidly growing porcine model arteries using quantitative angiography, growth pathology and histopathology was investigated. A description of the designed stent and the effects of its geometry and radial forces on the growing tissue is provided.

1.1 Coarctation of the Aorta (CoA)

Approximately 40,000 children in the US are born with a congenital heart defect (CHD) annually,[3] with the heart being the most commonly affected organ by birth malformations.[4] It has been estimated that 2.4 million children and adults in the US are currently living with CHD.[5] In particular, coarctation of the aorta (CoA) affects 4 in 10,000 children born in the US, accounting for 6%–8% of children with CHD. [6,7] A section of the descending aorta is narrowed in CoA, and this narrowing is usually located at the insertion of the patent ductus arteriosus (PDA) just distal to the left subclavian artery (Figure 1.1).[6,8] There are three hypotheses regarding development of CoA:[6] First, during development of aortic arch the tissue from the wall of the PDA blends into

the tissue of the aorta and when the PDA's tissue contracts, this blended tissue may also tighten and narrows the aorta and cause the coarctation of the aorta.[8,9] Second, during fetal life the area between left subclavian artery and the PDA is narrow due to the low blood volume that goes through it. After birth, normal volume of blood flow through the vessel and this area grows. Failure of this phenomenon can lead to formation of CoA.[8,10] Third, a small segment of the left dorsal aorta could form abnormally. Later, this narrow region moves cranially with left subclavian artery forming CoA.[8] CoA generally results in high ventricle pressure, exertional intolerance, heart failure with or without ventricular dysfunction and has a high morbidity and mortality if untreated.

Figure 1.1: Coarctation of aorta. In coarctation of the aorta a section of the descending aorta narrows, the narrowing usually located at the insertion of the patent ductus arteriosus (PDA) just distal to the left subclavian artery

1.1.2 Current Treatment Options for CoA

Balloon angioplasty and stenting are the current transcatheter treatments for coarctation of the aorta (CoA) in children. With a 98% survival rate at a median follow-up of 4.8 years, surgery has been the "gold standard" treatment for infants with coarctation.[11] Nonetheless, surgery is associated with numerous risks, including operative and cosmetic morbidities and coarctation

reoccurrence.[12] Balloon angioplasty is an accepted technique for infants aged 1–6 months with discrete narrowing; however, this option has been associated with aortic wall damage, restenosis (11%) and aneurysm formation.[11,2] The efficacy of stent implantation in overcoming some of the limitations of balloon dilation has been reported for children more than 3-4 years of age.[13] Forbes *et al*. reported that stented patients had a significantly lower rate of acute complications than those who underwent surgery and balloon angioplasty.[14] Currently, no balloon-expandable or self-expandable stent has been specifically designed for pediatric applications, and patients who receive balloon-expandable stents usually require a planned reintervention owing to the lack of growth in the stents.[2,15] Therefore, a great need for a stent with a capability to self-grow or to be resorbed is warranted.[1] Bioresorbable stents have issues related to the effects of their degradation products on the vasculature so it is reasonable to consider a stent that can "grow with" an artery in a growing child.[1]

Although both Zilver stents (Cook, Bloomington, Indiana) and Wallstents (Boston Scientific, Marlborough, MA) have been used with some success in the pulmonary arteries of children with congenital heart disease, little is known about the effects of self-expanding stents on growing arteries. [16,17] Covered thoracic endografts have been previously shown to inhibit aortic growth but uncovered, lower radial force self-expanding stents have never been tested for their ability to grow with an artery.[18] In this study, nitinol self-expanding stents were designed, modeled and manufactured specifically for this application. Four self-expanding stents with a range of outward radial forces were then used to study the effects of stent geometry and force on the biology of rapidly growing arteries in porcine model.

1.2 Nitinol Stent

A stent is a tubular scaffold device made from either metal, alloy or a polymer that is designed to be inserted into a constricted vessel in different areas of the body to keep the vessel open and restore the flow.[19] Stents come in different material and shape and can be balloon expandable, self-expandable or bioresorbable.[20] Currently there are several different materials for stent making base on the required needs. Stainless steel, platinum-iridium, tantalum, cobalt-chromium, superelastic shape-memory alloys (Nitinol), biodegradable polymers and magnesium are to name a few.[1,2,21] Each of these materials has a specific constitutive behavior and consequently requires a specific innovation stent design. Super-elasticity and shape-memory are the two characteristics that can be utilized to create a stent that can expand by itself with no external force applied to it (Self-expandable). [22]

Nitinol is an alloy composed of nickel and titanium. Its corrosion resistance, biocompatibility, and fatigue resistance, shape memory, and superelasticity behavior makes it a great material for an implant.[22] However, its super elasticity behavior, stress hysteresis, and biased stiffness characteristics makes it an ideal material for a self-expandable stent. In the next few sections, we will explain some of Nitinol's characteristics.

1.2.1 Nitinol Superelasticity

Non-elastic material such as stainless steel or cobalt chromium alloy show different elastic deformation behavior compared to living tissue. There is a 1% limit for the strain for elastic deformation of such metals; elongation also increases and decreases linearly with the applied force. However, biological tissue like bone, hair and tendon exhibit more elasticity and deformation, in some cases up to 10% strain in a non-linear way.[23] In these types of materials, the strain is

recovered at lower stresses when the deforming stress is releases. Nitinol stress-strain behavior is similar to that of structures in the biological tissue as shown in Figure 1.2 than conventional metal materials. The loading and unloading cycle are characterized by pronounced hysteresis.[22] Because deformation of more than 10% strain can be elastically recovered, therefore nitinol can be considered a superelastic material, which makes it an ideal material for a self-growing stent. [22]

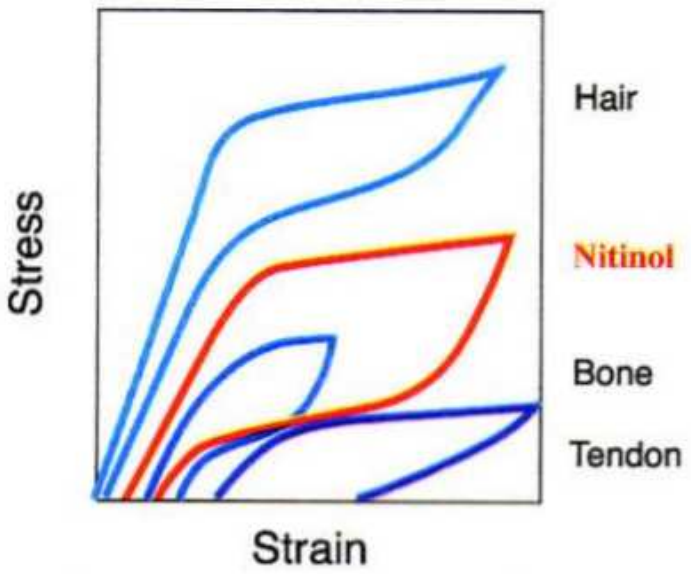

Figure 1.2: Biomechanical, behavior of nitinol with comparison to living tissue. Nitinol stress-strain behavior is like that of structures in the biological tissue.

1.2.2 Biased Stiffness

Biased stiffness is a Nitinol stent feature that results from the stress hysteresis of Nitinol, which plays a crucial rule for making a self-growing stent. [24] This concept is shown in Figure 1.3 and explained below, which demonstrates a schematic superelastic stress-strain curve for a Nitinol stent. This curve has both non-linear response and hysteresis and explains the chronic outward force and radial resistive force of a Nitinol stent, which form the basis for designing a self-growing stent.

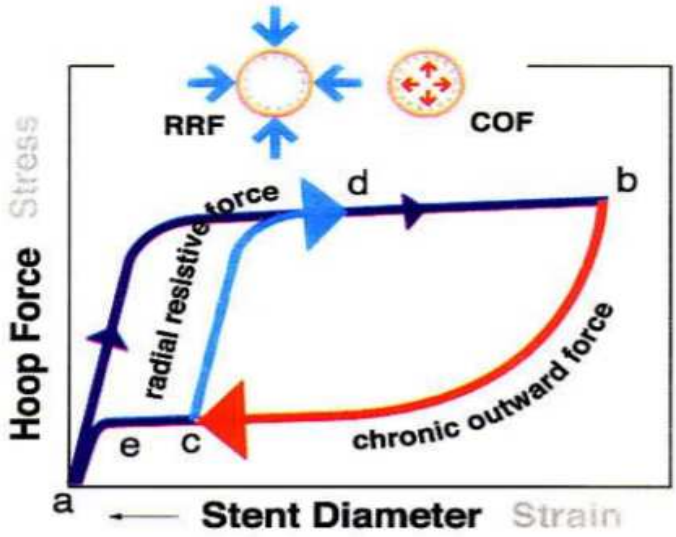

Figure 1.3: Schematic stress hysteresis and concept of biased stiffness. As demonstrated from point a to b, the stent crimped and placed inside a delivery system. Point b to c the stent delivered. At point c the stent is restricted by the vessel, but the stent exerts a chronic outward force to the vessel. If the stent compresses by an external force the stent will exert more force to resist the compression (point c to d) this force is radial resistive force**.**

Using this graph, Stoeckel et al., showed the cycle of crimping a stent into a delivery system, deploying it, and have it expand and interact with the vessel.[22] In this graph, the hoop force represents the stress and stent diameter represent strain. A large diameter stent (a) can be crimped into a small diameter (b) and be loaded into a delivery system (b) to fit into a vessel. Then, by releasing the stent into a vessel, we can make it expand from (b) until the movement is blocked by the vessel diameter (c). Because the smaller size of the vessel prevents the stent to expand to its full diameter, the stent exerts a low outward force, termed chronic outward force (COF). As shown in Figure 1.3, the chronic outward force stays constant even during the vessel growth and the increase in the vessel's diameter. If an external force compresses the vessel (i.e. elastic recoil of the aorta), the stents resists deformation with a greater force (radial resistive force; RRF), with forces dictated by the loading curve from point c to d. In such a way, the stress hysteresis and biased stiffness of Nitinol enables the design of a self-expanding stent, meaning that the stent

exerts outward force if it is placed in a small vessel and will expand with the growth of the vessel through exerting constant chronic outward forces and also resists deformation by applying radial resistive force.[22]

1.3 Vascular Injury and Remodeling Process

The intima, the media, and the adventitia are the three different layers of all arteries. As shown in Figure 1.4, the internal elastic lamina (IEL) separates the intima from the media and the external elastic lamina (EEL) separates the media from the adventitia.[25] The intima is the most inner layer of the arterial vessel wall, it consist of a layer of endothelial cells which have a direct contact with blood. The media is in the middle between the intima and the adventitia and the adventitia is the outer most layer of the vessel. Each of these three layers have their own function. The intima regulates the active response of the vessel through which pressure regulating agents reach the media, also it can produce nitric oxide to control the vascular tone, which relaxes smooth muscle cells in the media. The media consists of smooth muscle cells that are surrounded by an extracellular plexus of elastin and collagen (type I and Type III) and an aqueous ground substance that has proteoglycans.[25] The role of the media is to adjust the volume of blood in the vessel by constant constriction and dilations. The outer most layer, the adventitia consists of fibroblasts, connective tissue, and perivascular nerves, and act as a protective sheath, preventing damages of the vessel due to an acute increase in pressure. [26,27]

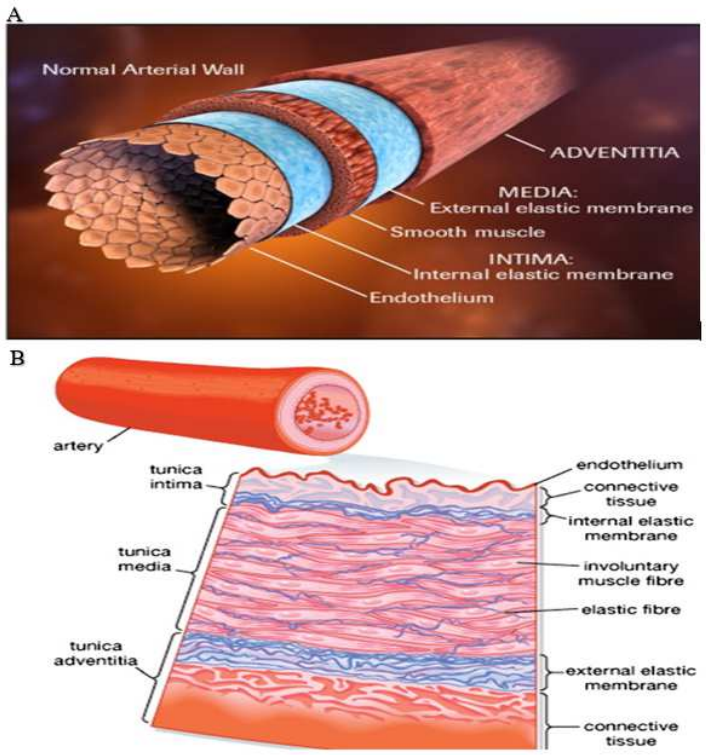

Figure 1.4: Schematic representation of distinct layers of arterial wall. (A) shows three distinctive layers arterial vessel: adventitia, media, and intima long with external (EEL) and internal elastic laminas (IEL). (B) Cross sectional view with the adventitia, media, and intima layers along with other different tissue layers.

Contiguous tissue tethering and internal blood flow put a significant mechanical stress on the arteries.[28] Also, if an implant such as a stent is implanted inside the artery, it could alter the biochemical and biomechanical properties of the tissue, triggering acute and chronic changes or remolding in the vessel.[25] Many different cell types that reside within the vasculature become involve in the complex and dynamic pathological process of the vascular remodeling.[29] Upon an injury to the arterial vessel wall, the remodeling of the vessel wall can be either constrictive or adaptive as Figure 1.5: Definition of arterial remodeling following injury shows it. Constrictive, inward, or negative remodeling can be accompanied by intimal hyperplasia in a patient with intima damage. Luminal narrowing or stenosis is the direct result of the constrictive remolding or intimal hyperplasia. On the other side, the vessel can go through adaptive, expansive, positive, or outward

remodeling which compensate for the formation of the neointima and it is believed to postpone the development of the stenosis, the flow limiting factor. [30]

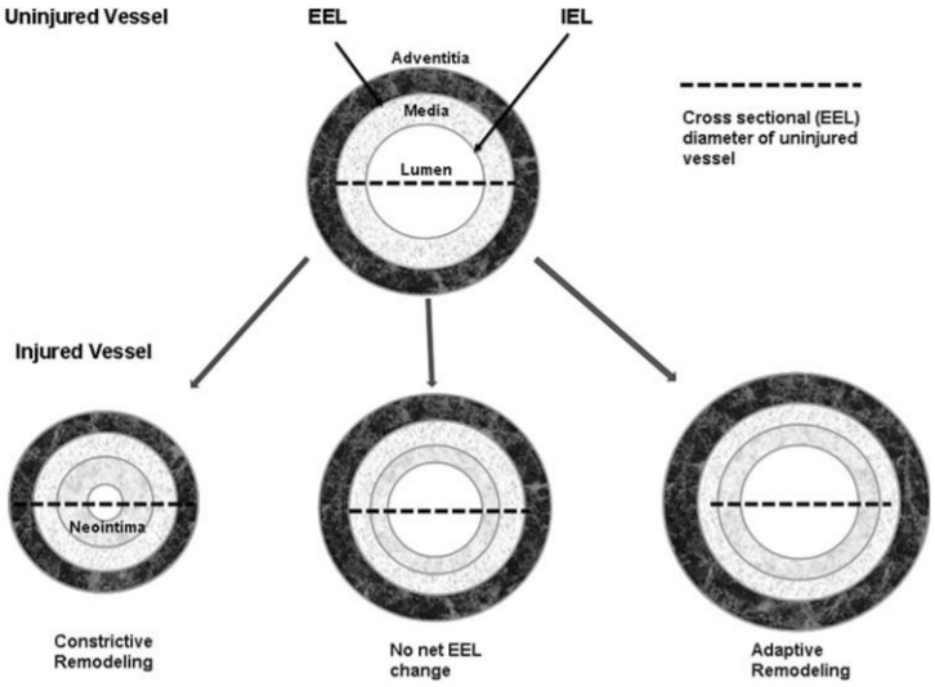

Figure 1.5: Definition of arterial remodeling following injury. The top image represents uninjured vessel. Images on the bottom show negative or constructive remodeling where the neointima will narrow the arterial lumen. The middle image shows no changes to the lumen vessel. Image on the right bottom shows adaptive or positive remolding where the lumen dilates and compensate for the formation of neointima, but the net lumen narrowing will not change. When vascular injury happens and initiate the remolding process

mesenchymal stromal cells (MSCs) reside within the adventitia and other types of cells such as macrophages will migrate and differentiate toward the smooth muscle cells in the intima and contribute to the neointima formation as shown in the Figure 1.6.[29] Aggregation of the neointima in the lumen can restrict the blood flow and cause stenosis.

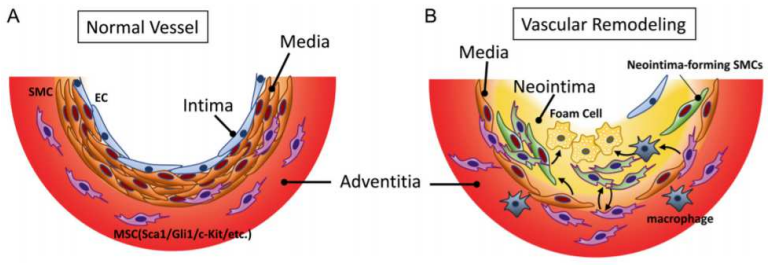

Figure 1.6: Normal vessel vs. vascular remodeling process. This figure shows normal vessel lumen on the left. Upon injury to the lumen, remodeling process starts, and many types of cells are moving toward the injury sight to start the remodeling process.

1.4 Histology

The study of the microscopic structure of tissues is called histology. In histology, advanced imaging techniques, such as electron microscopy or light microscopy, are used to analyze and identify the tissue and the structures present. In histology, samples can be specially processed and prepared for visualization of the structure and the disease. In, Figure 1.7 histology of the arterial vessel wall shows the intima, the media and the adventitia along with IEL and smooth muscle cells.

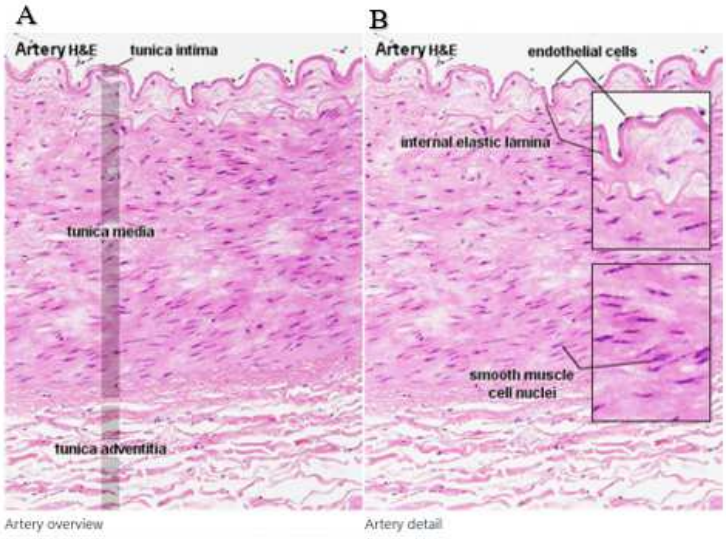

Figure 1.7: Histologic examples of artery. (A) shows artery overview with intima, media, and adventitia layers. (B) represent the artery detail with structure of endothelial cells, IEL and smooth muscle cell nuclei. Images with H&E staining. [31]

Generally, there are different techniques in the processing of the tissue for histology. The tissue processing methods include plastic and paraffin histology along with different staining techniques such as hematoxylin and eosin (H&E), Movat's Pentachrome and Elastin Trichrome staining to analyze and visualize the tissue structure. In each process, the tissue is fixed using dehydrated techniques using alcohol. Then the tissue is embedded in either plastic or paraffin resin. Each sample then is sectioned using a grinding method or cutting method using a sharp blade. In plastic histology processing each section can be cut in 19 to 90 microns vs. in paraffin histology the tissue embedded in paraffin, which is similar in density to tissue can be sectioned at anywhere from 3 to 10 microns. Analysis can be performed after staining methods under a microscope. Usually H&E staining can be used to examine cellular type and quantity and fibrin deposition, while Trichrome Elastin staining can be used for observing any type of injury in the lumen of a vessel, the media, or EIL, EEL and other structures.

1.5 Summary of Chapter 1

At the beginning of this chapter the limitation (lack of growth) in the current stents for use in rapid growing children was discussed, and a great interest among pediatric community in stents that can grow with an artery or be resorbed. Coarctation of the aorta (CoA) is a congenital disease in children that can potentially benefit from self-growing stents. Stenting as a superior solution compared to balloon angioplasty and surgery for fixation of CoA was discussed. The properties of Nitinol, an alloy that can be used for self-expanding stents due to some of its unique characteristic properties such as superelasticity, and biased stiffness was discussed. Also, the vascular injury and its remodeling process after the injury, such as negative and positive remodeling was reviewed. In addition, histology and several types of processing and staining that are utilized in the science of histology for microscopic evaluation of the tissue structure was mentioned.

CHAPTER 2: LITERATURE REVIEW

Currently, there is little information available on the effect of stent radial force on the rapid growing arteries in pediatric patients.[32] However, there are a good number of studies focusing on the adult abdominal stent grafts, coronary and peripheral artery stents, exhibiting the effect of stent and stent grafts, and their radial forces on the vascular biology.[31,32,] Nevertheless, none of the investigators looked extensively at the large growth of small crimp profile bare metal stents and, particularly, did not design a stent that can grow with the small rapid growing arteries for use in the pediatric endovascular applications. An extensive literature search was performed and the findings from a few key sources are summarized in two categories below.

2.1 Endovascular Stenting and the Effect of it on the Arterial Wall

Siegenthaler et al., evaluated the growth and the effect of the stent grafts covered with polyester on the thoracic aorta in young piglets. [18] The authors concluded that the stent graft may inhibit growth of the nonatherosclerotic normal aorta and lead to intimal hyperplasia and focal fibrosis in the inner media adjacent to the stent. Siegenthaler et al., proposed several reasons for their finding, including vascular hemodynamics and the change in pressure profile on the arterial wall due to the polyester covers on the stent. Polyester covers can absorb the most mechanical forces on the arterial lumen, leading the change in the wall stress and less pressure contact and reduce the pulstality exposure of the aortic wall. Another problem with the stent graft is the potential to cover the side branch vessels during deployment, usually the subclavian artery ostium in CoA.[2] In conclusion, the authors suggested that more study should be conducted to evaluate stent and stents grafts in growing aorta.

Cheung et al., reported on the early and the intermediate-term follow-up results of Wallstent (Boston Scientific, Marlborough, MA) a self-expandable stent implanted in children

with congenital heart disease. [17] The Wallstent has been widely used by interventionalist in Europe for adult patients with the iliac and femoral arterial stenosis.[33,34] In two different centers, from 1993 to 1997, Cheung et al., implanted Wallstents in 20 children with average age of 10 years old and an average weight of 30.5 kg. The results showed immediate expansion of the stents and reduction of the pressure gradient in the patients. However, the authors observed migration in two of the optimally positioned stents within 24 hours of implantation, along with significant neointimal ingrowth in 28% of the patient at the mean follow-up duration of 8.1 months, which contrasts with the experience of patients with Palmaz stents where the significant restenosis is at 3%.[35,36,37] Cheung et al., suggested the thrombogenicity of the stent could be due to the design of the stent, woven mesh with expanding radial force, versus Palmaz's rigid slotted tubes with smooth and even surface. The authors also reported the stent did not pace with the growth of the vessel, therefore limits it use in young children.

Hong et al., performed an experimental study with CardioCoil (TM), a self-expanding stent in the coronary artery of pigs, for a duration of six months.[38] The authors performed angiographic and histologic analyses to evaluate the deployment characteristics, patency rates, and neointimal response. The neointimal responses in this study were not significant and the stents were patent through the survival period up to 6 months. The stents expanded over time; the diameter of the stents at the time of implant was 2.85 ± 0.78 and at the follow-up showed to be 3.24 ± 097mm. Hong et al., observed penetration of most of the stent's struts into the adventitia. The authors concluded that the self-expanding stent is related with favorable deployment characteristics and potency rates, although appropriate sizing is more crucial than with balloon-expandable stents. More importantly, Hong et al., concluded that, unlike balloon-expandable stents, there is a

dissociation between major vessel injury by the chronic strut expansion process and the neointimal reaction.

Freeman et al., explored the effect of the stent forces in vascular stenosis and remodeling by placing stainless steel stents with three chronic outward forces (COF)—3.4N, 16.4N and 19.4N—in the iliac arteries of juvenile porcine models for a duration of 30 days to explore and develop an equation for identifying the optimal stent force.[39] The results of the authors' investigation revealed a significant increase in the total thickness and neointimal hyperplasia in the stents with higher COF than the lower ones, which corresponds with several other similar findings.[40,41] Freeman et al., concluded that the geometry, structure, and mechanics of the target vessel need to be considered when a stent is designed and, in order to achieve maximum dilation, stents should not produce stress in the vessel wall greater than the end of the transitional domain of the vessel's stress-strain curve. The authors suggested that their findings could be extremely useful in the vascular stent developments.

In a 180-day study, Zhao et al., explored late stent expansion and neointimal proliferation of over-expanded Nitinol stents in the peripheral arteries.[42] The authors used Nitinol self-expanding stents with a maximum diameter of 8 mm and length of 28mm. Zhao et al., implanted the stents into the iliofemoral arteries of Yucatan swine. Due to variations in target artery size, the stent-to-artery ration ranged from 1.2:1 to 1.9:1 and the effect of stretching investigated. the authors observed high stent diameter-to-artery ratio, which resulted in overstretching of the arterial wall. Finally, Zhao et al., reported that the overstretching of an artery can lead to medial injury, and medial injury will cause a profound long-term histological response, including significant neointimal proliferation. Saguner et al., found that stents (5-6mm in diameter) constrained by their target artery at implantation expanded over time to near their nominal diameter within five

months.[43] Like the previous study, severe oversizing determined as an oversizing ratio (1.4:1) resulted in significant neointimal proliferation and in-stent restenosis.

Barth et al., performed a side-by side comparison of three current stents in the market that are substantially different in their physical characteristics: Palmaz stent, Strecker stent and Wallstents.[44] Palmaz is the most rigid stent and has a very high resistive outward force in vitro in comparison to the Wallstent. The Strecker is made of tantalum, has the lowest resistive force of the three, and is very flexible and maneuverable. Among the three, the Palmaz stent is the nonelastic one with a lower profile, the Wallstent is fully elastic with a higher profile, and the Strecker stent is elastic to a lesser degree with a higher profile.[45,46] All stents were implanted into canine external iliac and the flexing portion of the proximal femoral artery of dogs. Angiographic images of mid-stent luminal diameters instantly after placement of the stent and at follow-up, as well as mid-stent cross-sectional areas of neointima were compared by the investigators for significant differences. Barth et al., concluded that the Strecker stent with a high profile and low resistive force is affected by the vascular wall recoil and caused the formation of a greater amount of neointima in comparison to the lower profile high resistive force Palmaz stent and Wallstent. Medial atrophy is pronounced outside the latter two stents. The authors found that in the flexing arteries, the rigid stent can penetrate through the vascular wall.

Sakakoa et al., studied the vascular response of bare Nitinol stent in porcine femoral and femoropopliteal arteries.[47] The authors implanted bare Nitinol stents in non-flexing femoral arteries (FA) and flexing femoropopliteal arteries (FPA). The authors performed quantitative angiography and histopathology at one and three months to evaluate and assess the biological response to the two devices. Sakakoa et al., observed an increase in the neointimal area in FPA in comparison to FA and late lumen loss in FPA than in FA. The authors concluded that repetitive

interaction between the stent and the vessel wall during dynamic vessel motion could affect vascular responses.

Several clinical studies reported the use of different types of stents for fixation of the CoA. We reviewed a few of them and some of them are summarized here. Haji-Zeinali et al., used currently in the market self-expandable Nitinol aortic stents in eight hypertensive patients (age 15 to 27 years) with coarctation of the aorta.[48] The authors showed that after implantation of the stents, the mean systolic gradient decreased significantly. Haji-Zeinali et al., also reported that Nitinol stents were easier to deploy and conformed better to the aortic anatomy compared to balloon-expandable stents. Finally, the authors found that Nitinol stents could be used to treat the coarctation of the aorta safely and effectively; these types of stents had similar efficacy in reducing coarctation of the aorta as surgical repair. Although Haji-Zeinali used these stents in adult patients, we believe the application of Nitinol self-expanding stents can be extended to the pediatric applications and especially neonatal applications for the reduction of CoA.

Bugeja et al., used a stent in neonatal for fixation of the coarctation of the aorta. They reported a case of a severely-ill newborn with complex coarctation, multiorgan failure, disseminated intravascular coagulation and oedema, who had to go through an emergency stenting procedure on the tenth day of her life.[49] Since there are no designed stents for neonates, the authors used an off-label used bare metal adult coronary stent (Bitonal Pro Kinetic 3.5/13 mm). With a fast pace of growth in the neonates, Bugeja et al., placed the stent temporarily and planned a surgical procedure to remove the stent and fix the coarctation surgically. This study clearly demonstrated the need for a stent that can be placed in patients and grow with them to eliminate or reduce the future interventions.

2.2 Designing of an Optimum Stent

Prior to designing the stent for this investigation, the most used stents in the congenital heart disease field was reviewed. Stents can be categorized based on their delivery method: balloon-expandable or self-expandable stents.[2] Balloon expandable stents (BES) are inflated with a balloon and their size is determined by the diameter of the balloon that they are inflated with. These stents are mostly rigid with high external outward force. Self-expanding stents (SES) are more flexible and restrained within a covering sheath, and by removing the sheath and uncovering the stent; the stent expands.[1] The common materials used to make stents are stainless steel (316L), platinum-iridium, Nitinol, cobalt-based alloys, titanium, and tantalum, along with some biodegradable, bioresorbable materials such as magnesium and resorbable polymers.[1,2,50] Because of anticipated growth in children, self-expandable stents are ideal to be used in children.[1,2] There are several varieties of stent design that have been used in congenital field, including mesh, coil-loop, ring and slotted tube, closed cell, open cell, and welded tube.[1,2] Here some of the investigation that others did to create an optimum stent is reviewed.

Peters et al., described the desirable features for an ideal stent design in pediatric cardiology.[2]

1. lower stent crimp profile with
2. high trackability
3. flexibility to navigate steep curves
4. good radio-opacity
5. MRI compatible
6. minimal foreshortening
7. enough radial strength to keep the lumen open

8. high flexibility with good fatigue performance
9. biocompatibility with resistance to thrombus formation and corrosion
10. prevention of plaque protrusion
11. avoidance of neointimal proliferation
12. round and soft edges for avoidance of intimal damage
13. possibility of future redialation to expand to full diameter
14. wide struts to maintain blood flow to jailed vessel branches
15. retrievability and possibility of repositioning

Such a stent is not yet available that combines all these requirements, however in this investigation it was tried to address some of these features in the designed stent. Sullivan et al., investigated the effect of the endovascular stent strut geometry on vascular injury, myointimal hyperplasia and restenosis.[51] The authors used a Palmaz stent with rectangular struts and smooth corners and a novel stent with thicker struts and sharper corners to induce larger wall stress concentrations in a 90 days study. Sullivan et al., found that the thicker strut and sharper corners resulted in a statistically higher incidence rate of deep vascular injury compared to the Palmaz stent. As a result, a higher restenosis rate observed with thicker and sharp corner struts. At the end of their study the authors concluded that maintenance of an intact internal elastic lamina (IEL) is crucial to prevent myointimal hyperplasia and restenosis in stented porcine iliac arteries. Sullivan et al., also found that superficial injury elicits a response that is independent of the stent strut geometry and vessel wall compression. Stent strut profile may, however, increase local vessel wall stress concentrations, leading to IEL rupture and an exaggerated response injury. Therefore, when stents are designed, extra attention should be given to the strut geometry.

Bedoya et al., designed some generic stent models that represent the characteristics present commercially available stents.[19] The authors deployed each stent in a homogeneous nonlinear hyperplastic artery model and evaluated them using commercially available finite element analysis software. Using computer simulation modeling Bedoya et al., suggested that stent designs incorporating a large axial strut spacing, blunt corners at bends, and higher amplitudes exposed smaller area of the artery to high stresses, while keeping enough radial force that is enough to keep the lumen open and restore flow. The mentioned articles were reviewed along with several others and they were used to characterize and design the self-expanding stent for this investigation.

2.3 Summary of Chapter 2

In this chapter, endovascular stenting and its effect on vascular arteries as well as how to design an optimum stent was reviewed. A study summarizing the stent grafts that inhibited the growth of the arteries in rapid growing piglets was investigated. Also, clinical studies in children was reviewed and reported that a commercially available self-expanding stent grew with the artery; however, stents migrated in two cases and in other cases these stents caused significant stenosis and obstruction of the lumen in the patients. The effect of the chronic outward force on the lumen of the artery and how over stretching the arteries can cause neointima proliferation was reviewed. In addition, several papers discussing the requirements of a stent for pediatric application as well as how to design an optimum stent that can distribute the force and minimizes the damage to the arterial wall was reviewed. Utilizing all the findings we attempted to design a stent that can grow with small rapid growing arteries and induces the least response.

CHAPTER 3: MATERIALS AND METHODS

3.1 Test Articles

In this investigation the test articles are novel designed self-expandable Nitinol stents. The benefits of stenting for CoA was discussed earlier. Nitinol material characteristics such as corrosion and fatigue resistance, biocompatibility, shape memory and its super elasticity behavior, and biased stiffness characteristics was utilized to create a self-expandable test articles that can grow with rapid growing arteries for this investigation.

3.1.1 Stent Characterization and Design

It was tried to fulfill many technical requirements in the design of the novel self-expanding Nitinol stent. These requirements were both mechanical and requirements that effect the biology of the surrounding tissue. For this investigation, the optimization of the mechanical properties of the stent, focused on some of the important requirements that is mentioned in other literatures too[2]:

1. The ability to crimp extremely low to 5-6 Fr
2. Provide adequate radial force to keep the lumen of the vessel open,
3. Overcome the elastic recoil of the artery,
4. Minimizing the damage to the vessel, and local biological response to the product
5. Flexible and be able to navigate to steep curves
6. Good radio-opacity
7. MRI compatible and
8. Minimal foreshortening are a few of them. The ability of the stent to expand to 20mm was also a priority in the design of the stent, along with the ability to post balloon dilation, if needed.

High stress forces in an arterial wall induced by a stent can have an adverse effect on the surrounding biology, causing stenosis or aneurysm.[52,53] Bedoya et al., found that stent designs

incorporating large axial strut spacing, blunt corners at bends, and higher amplitudes exposed smaller regions of the artery to high stresses, while exerting sufficient radial forces to keep the lumen open.[19]

Four potential pediatric self-expanding stent designs with varying numbers of struts, width, thickness, shape, length and architecture were created using Creo Parametric CAD (formally pro/ENGINEERING, PTC Inc. Boston, MA) as shown in Figure 1. The crimp profile of each design was simulated using SIMULIA Abaqus FEA software (Abaqus Inc. Johnston, Rhode Island). Through crimp profile simulation, each design underwent iterations by adjusting the number of struts, width, and thickness in order to achieve the following pre-determined traits: crimp profile of < 6Fr, unconstraint diameter of 20mm, and length of 15 to 20mm with a radial force able to withstand vessel recoil after angioplasty. Radio-opacity for visualization under fluoroscopy was also a required but was not simulated. A stent design with a single row, high amplitude, and low number of struts was selected that could be easily crimped to <6 Fr as indicated by an arrow in Figure 3.1. This design served as the basis for sub-selection of specific candidate stents.

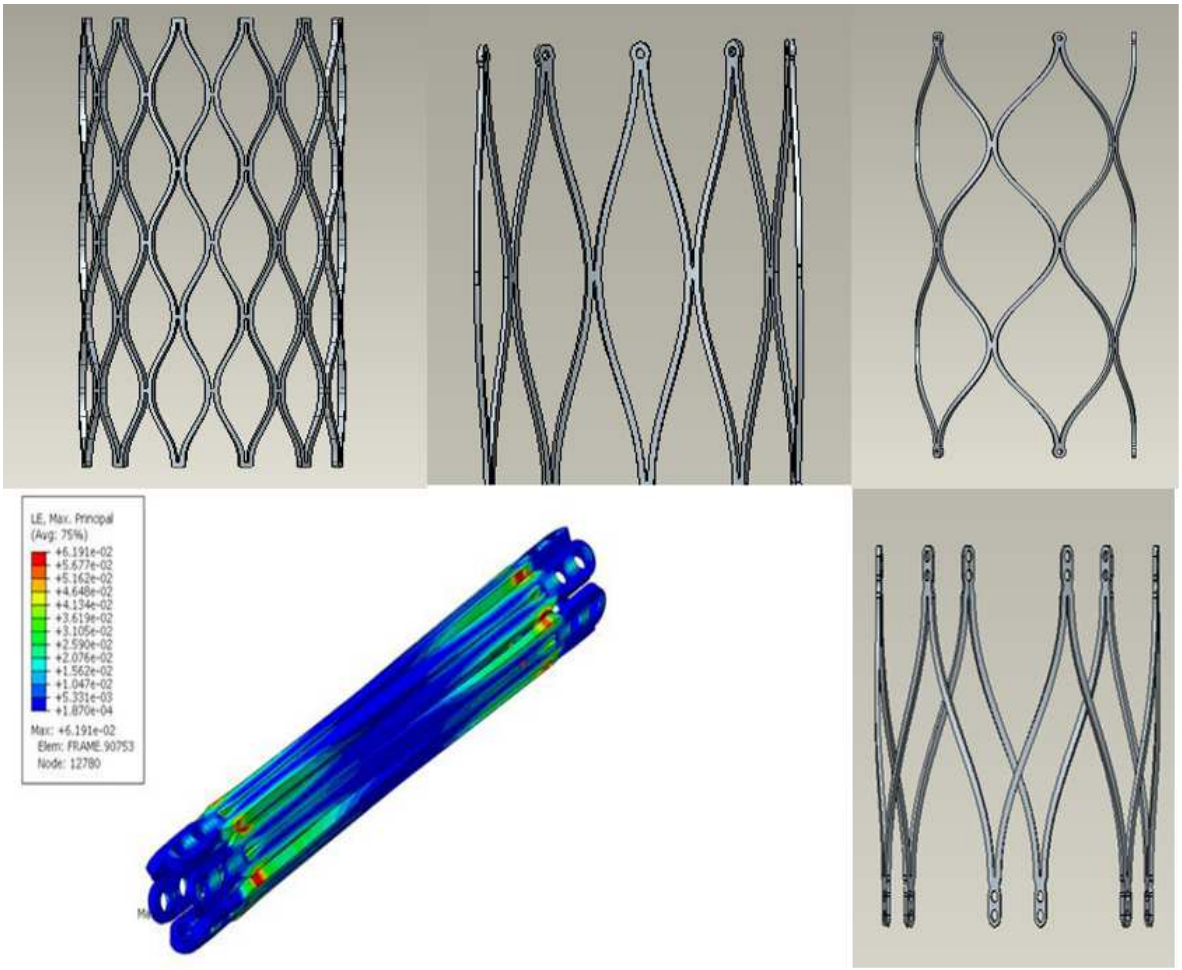

Figure 3.1: Designed stents and sample of computer simulations to obtain crimp profile. Stents with different strut's width, thickness, shape, length and architecture. A sample of crimp profile simulation is presented.

3.2 Stent Fabrication

The strut's width and length of the selected design were adjusted to create four stents with different chronic outward forces (COFs). Each stent was laser cut (Amada Miyachi America laser cutter, Monrovia, CA) from a 0.31-mm-thick Nitinol tube with a 10-mm diameter (Vascotube GmbH, Birkenfeld, Germany). Each stent was expanded to 20 mm using a 20-mm mandrel and shape-set using automated salt bath equipment at 500°C for 5 min. Subsequently, stents were ultrasonically cleaned and electropolished using an electrolyte solution (methanol, nitric acid

[7+3]) at -33±5°C. Figure 3.2 illustrates the parent design along with the four stents generated from it.

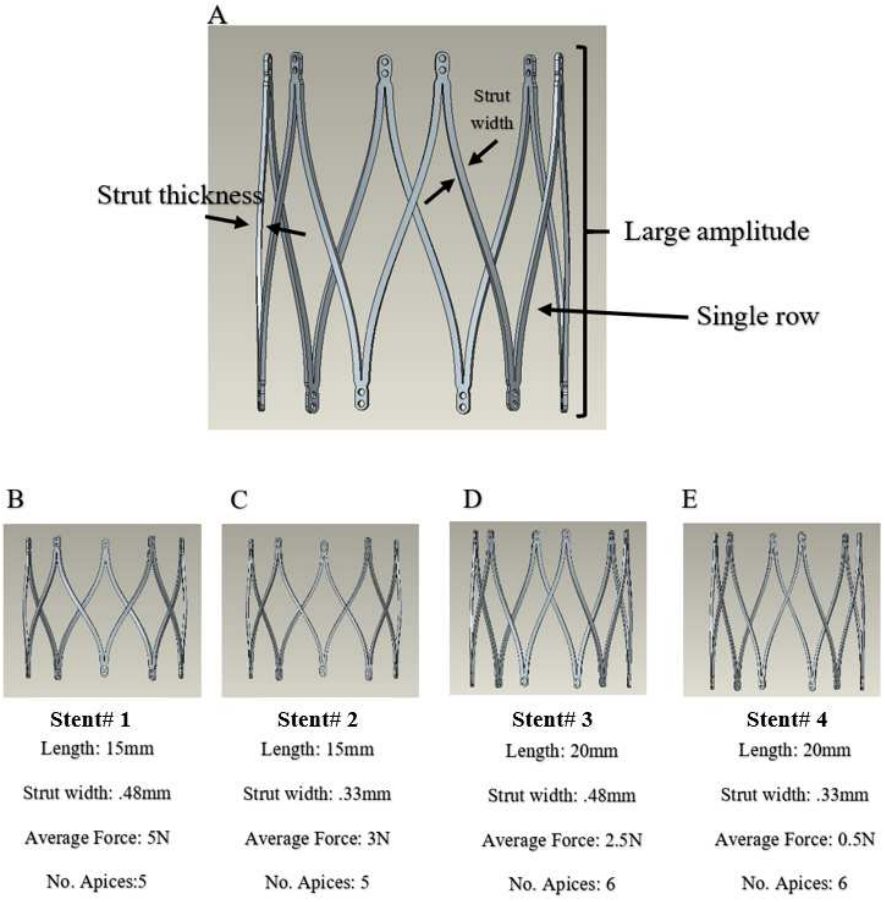

Figure 3.2: (A) Designed self-expanding growth stent with a single row and large amplitude (parent stent). The strut thickness is 0.27 mm for all stents. (B) Stent 1 (C) Stent 2 (D) Stent 3 (E) Stent 4.

In vitro testing was performed to determine radial force as a function of diameter as well as to confirm crimping and radio-opacity. Each stent's COF was characterized in a radial force tester (Machine Solutions Inc, Flagstaff, AZ). This equipment measures and records COF during expansion and radial resistive force during compression and generate a hysteresis curve (force vs.

diameter) as shown in Figure 3.3. Using the plots, the exact COF or resistive force of the stent at a specific diameter can be measured. Stents were crimped using a crimper (Edwards Lifesciences, model 9600, Irvine, Ca) and by hand and tested to fit easily into a 6 Fr lumen. Stents were radiographed under fluoroscopy settings of 80±5 Kv to confirm adequate visualization under fluoroscopy.

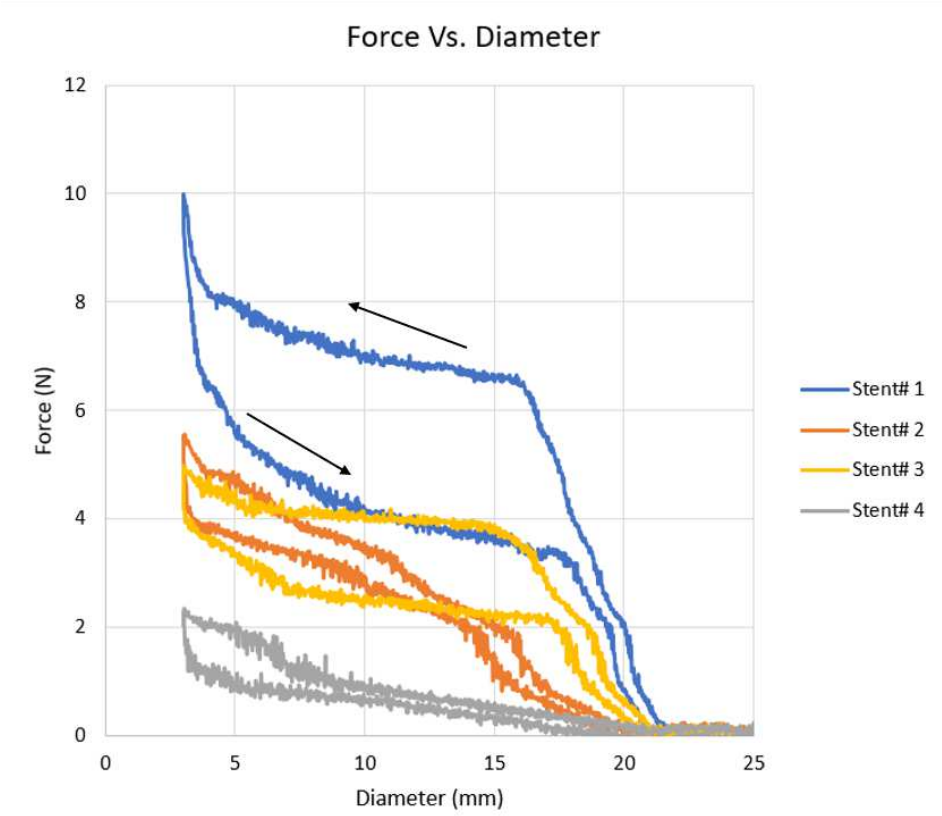

Figure 3.3: Hysteresis curve force versus diameter for each Nitinol stent. The arrows indicate the hysteresis direction.

The surface area of each stent was measured using Cero Parametric 3D modeling (ProEngineering) software. Average pressures in Kilo Pascal for each stent calculated using average radial force and the surface area. The stent specification along with calculated pressures in KPa are shown in Table 3.1.

Table 3.1. Prototype stent specifications

Stent Specification	Length	Strut width	Strut thickness	Crimp profile	Full diameter	Radial force		Surface area (mm^2)	Pressure (KPa) Ave
						Max	Ave		
Stent# 1	15mm	0.48mm	.27mm	<6F	20mm	10N	5N	103.33	40
Stent# 2	15mm	0.33mm	.27mm	<6F	20mm	5N	2.5N	76.37	30
Stent# 3	20mm	0.48mm	.27mm	<6F	20mm	5.8N	3N	132.24	20
Stent# 4	20mm	0.33mm	.27mm	<6F	20mm	2.5N	0.5N	96.77	5

3.3 Animal Model

Porcine is the most common animal model used to investigate stenting in aortas due to the anatomical similarity to the human, A porcine model was used for this investigation.[54] We assessed the vascular responses, after implantation of the self-expanding stents in the porcine abdominal aorta and the iliac for a duration of 90 and 180 days.

3.3.1 Implant Procedure

Three-month-old female pigs (*Sus scrofa)* weighing approximately 50 kg were used. Animals were anesthetized with a mixture of tiletamine-zolazepam (4.4 mg/kg), ketamine (2.2 mg/kg) and xylazine (1.1 mg/kg) given intramuscularly. The animals were intubated and maintained on isoflurane in oxygen to effect. A 5 Fr pig tail angiographic catheter (Cook, Bloomington, Indiana) was inserted in the descending aorta and contrast angiography was performed (GE Innova 3100IQ; GE Healthcare, Waukesha, WI). The arterial diameter prior to implantation was measured using measurement tool feature of GE software Innova 3100IQ version IGS5_1.0. (GE Healthcare, Waukesha, WI). A 12-Fr Cook sheath was modified using a 10-Fr Nylon tube (PN E180117-4) for

a delivery system. Pusher stylets were prototyped using Nylon tube (PN E180117-5) and a Tuohy-Borst adapter (PN 80330; Qosina, Ronkonkoma, NY) and used to push the stents out of the delivery systems. A total of 14 stents were implanted using right femoral access. Animal A was implanted with Stent# 1 and 2 in the abdominal aorta for a duration of 90 days. Animal B, C, and D were implanted with Stent 1 through 4 in the abdominal aorta for a duration of 180 days. In each of these animals, Stent# 1 was implanted most proximally followed by Stents# 2, 3, and 4 in this order from proximal to more distal aorta/ iliac (Figure 3.4). Final angiography was performed, the lumen dimeter of stented and non-stented arteries were measured as above.

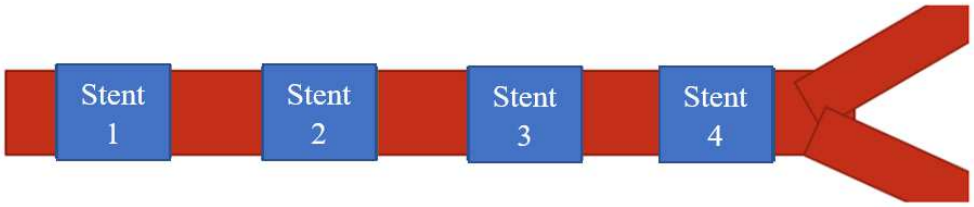

Figure 3.4: Implants configuration in abdominal aorta for 180 days study durations. Stent# 1 implanted in the proximal side of the abdonimal aorta followed by Stent# 2, 3 and 4 the distal side. In 90 days study only Stent# 1 and 2 were implanted.

3.3.2 Explant Procedure

Either 3 months or 6 months after implantation, each animal was re-anesthetized as described above and angiography was performed. The lumen diameters of stented and non-stented arteries were measured as above to assess the luminal patency and diameters of the stented arteries. Finally, the animals were euthanized with euthasol (pentobarbital sodium and phenytoin sodium) 1 ml/4.5 kg IV. A complete necropsy was performed. The stented vessels were isolated, radiographed, photographed, and placed in 10% buffered formalin. The Weight at implant, at explant, and duration of the study for each animal is summarized in Table 3.2

Table 3.2. Duration and the weight of animal at implant and explant.

Porcine #	A	B	C	D
Duration	**90 days**		**180 days**	
Weight at implant(kg)	50	53	51	51
Weight at explant (kg)	100	150	128	138

3.4 Histology

All histopathology analysis was performed at CVPath Institute Inc (Gaithersburg, MD). Before processing for the histology, digital photograph was taken (Canon Rebel XSi) of the vessel and obtained Faxitron digital radiographs in the anterior-posterior and the lateral views. The radiographs demonstrated four nitinol bare metal stents, two measuring 15 mm long and two 20mm long and 10 to 18 mm in greatest diameter for 180 days study and two stents each 15mm length and 12 to 13mm in greatest diameter for 90 days study. An approximate 5 mm non-stented segment was present between the stents. The stents were submitted for embedding in Spurr resin and sectioning by the Exakt method. Proximal, mid, and distal non-stented aortic segments were submitted for paraffin embedding and routine histologic sectioning.

3.4.1 Plastic Histology

To prepare the samples for plastic histology the stented aortic segments were dehydrated in a graded series of ethanol and infiltrated and embedded them in Spurr resin. After polymerization, transverse sections were sawed approximately 4 millimeters in thickness from the stents. Final slides were grounded from each of the plastic blocks to a final thickness of 19 to 90 microns using EXAKT Linear Grinding Technology. Each sample then polished and stained ground sections with hematoxylin and eosin (H&E). The mid-section of each stented segment was

stained with Trichrome staining. All sections were examined by light microscopy for vessel wall integrity and inflammatory response.

3.4.2 Paraffin Histology

Proximal, mid, and distal non-stented aortic segments were submitted for paraffin embedding and routine histologic sectioning. After dehydration in a graded series of ethanol and infiltration with paraffin, the transverse sections for each segment were cut. Each block was sectioned at 4-6 microns and mounted them onto slides and stained with hematoxylin and eosin (H&E) and Movat's Pentachrome (for 90-days data only). All sections were examined by light microscopy for vessel wall integrity and inflammatory response.

3.4.3 Quantitative Histomorphometric Analysis and Histopathology Analysis

Morphometric analysis was conducted on each stented segment, and quantitative assessment was performed to determine the morphometric effects of treatment. For the performance measurements, histological sections were analyzed using digital planimetry with a NIST-traceable calibrated microscope system (IP Lab software, Rockville, MD). Morphometric measurements included the luminal area; internal elastic lamina (IEL) and external elastic lamina (EEL) layers of the stented vessel; and neointimal thickness. From the above parameters, the following parameters were calculated:

- Neointimal area = IEL area − luminal area
- Medial area = EEL area − IEL area
- Percent area stenosis = $\left[1 - \left(\frac{Luminal\ area}{IEL\ area}\right)\right] \times 100$

For the comparison of neointimal organization and healing, semi-quantitative ordinal data on each stent section were collected. Histological parameters included fibrin deposition, hemorrhage, inflammation, giant cell reactions, and granulomas. Endothelial coverage was

visually estimated, and device safety, overall injury, inflammation, and fibrin deposition for each section were scored using the method described by Schwartz et al.[9] The relationship between the stent COF and the histopathology results was then assessed. To evaluate device safety, we scored an overall injury, inflammation, and fibrin deposition value for each stented section according to the scoring scheme shown in Table 3.3.

Table 3.3. Semi-quantitative evaluation of pathologic changes in vessels

Attribute	Score	Description of Assigned Weight
Injury Score (Using the method described by Schwartz et al.,[55])	0	Internal elastic lamina (IEL) intact, endothelium typically denuded, media may be compressed but not lacerated
	1	IEL lacerated, media typically compressed but not lacerated
	2	IEL lacerated, media visibly lacerated, external elastic lamina (EEL) intact but may be compressed
	3	EEL lacerated, typically large lacerations of media extending through EEL, struts sometimes residing in adventitia
Neointimal Inflammation Score	0	<25% struts with few than 10 inflammatory cells
	1	Up to 25% struts with greater than 10 inflammatory cells
	2	15-50% struts with greater than 10 inflammatory cells
	3	>50% struts with greater than 10 inflammatory cells
	4	2 or more struts associated granulomatous inflammatory reactions
Fibrin Score	0	No fibrin is appreciated (or only small strands)
	1	At least 25% of struts involving confluent fibrin that surrounds up to 25% of the strut circumference
	2	At least 50% of struts involving confluent fibrin that surrounds >25% of strut circumference
	3	All struts with confluent fibrin surrounding >50% of strut circumference with 25-50% of struts, AND extension between struts or bridging
Adventitial Inflammation Score	0	No inflammation to minimal interspersed inflammatory cells anywhere in the adventitia
	1	Mild peripheral inflammatory infiltration or focally moderated in <25% of adventitial area
	2	Moderate peripheral inflammatory infiltration or focally marked in 25-50% of adventitial area
	3	Heavy peripheral inflammatory infiltration or focally marked in >50% of adventitial area

Injury score, neointimal inflammation score, fibrin score and adventitial inflammation score and the description of assigned weight is explained in this table.

3.5 Summary of Chapter 3

In this chapter, it was discussed how the novel stent was designed, manufactured and characterized, as well as the implant and the explant procedure for the study. The histology, with different processing and staining techniques; morphometric analysis on each stented segment; and the quantitative assessment to determine the morphometric effects of the treatment was also discussed.

CHAPTER 4: RESULTS

Hysteresis curves were generated for the four-candidate stent as shown in (Figure 3.3). Figure 3.2 provides an overview of Stent# 1-# 4. Stent#1 and Stent# 2 were both shorter, 15 mm, and had 4 zigs/apices. Stent#1 was the highest radial force stent with an average COF of 5 N secondary to increased strut thickness of 0.48 mm versus 0.33 mm for Stent# 2. Similarly, Stent#3 and Stent# 4 were longer (20mm) and had lower average outward forces. Stent# 3 had a higher COF (2.5 N) than Stent# 4 secondary to increased strut thickness of 0.48 mm versus 0.33 mm for Stent#4.

A total of 14 self-expanding nitinol stents were implanted in four 3-month old pigs weighing approximately 50 kg for a duration of 90 and 180 days. All animals survived until the scheduled necropsy without any abnormalities attributable to the implanted stents. The animals grew to an average weight of 100 and 139 kg at 90 and 180 days, respectively. Angiography revealed the patency of all stented vessels and stent expansion in the arterial lumen beyond the size of the adjacent native vessel. In Animal A, Stent #1 and Stent # 2 were implanted for 90 days. In animal B, all four stents were implanted, and one stent was implanted inside the iliac artery. In Animal C, Stent# 1&2 and Stent# 3&4 overlapped. All other stents were implanted at appropriate locations. Table 4.1 represents the vessel lumen diameter at the time of implant and the amount of COF obtained from hysteresis plots of each stent, along with final diameter of stents, percent growth and duration of study.

Table 4.1: Vessel and final stent diameter, stent COF, final stent diameter, % growth and duration of implant time.* The overlap stents, Stent 1&2 and Stent 3&4. ** Only Stent 1 and 2 were implanted in Animal A.

Stent# 1

Animal	Vessel diameter at implant (mm)	Stent COF (N) at implant	Final stent diameter (mm)	% Growth	Duration Days
A	9.8	4.10	13.3	36	90
B	11.1	3.98	14.5	31	180
C*	10.0	6.63	16.9	69	180
D	15.0	3.54	18.9	26	180

Stent# 2

A	9.8	2.00	13.0	33	90
B	10.6	2.55	14.0	32	180
C*	X	X	X	X	180
D	13.7	2.31	17.2	25	180

Stent# 3

Animal	Vessel diameter at implant (mm)	Stent COF (N) at implant	Final stent diameter (mm)	% Growth	Duration Days
A**	X	X	X	X	X
B	10.6	2.73	14.9	41	180
C*	7.5	5.96	14.2	89	180
D	14.6	1.87	17.2	21	180

Stent# 4

A**	X	X	X	X	X
B	4.5	0.92	10.4	131	180
C*	X	X	X	X	X
D	13.9	0.34	18.1	30	180

4.1 Vessel Growth Summary

The changes in the angiographic stent diameter (absolute growth) for the stented vessel at 90 and 180 days after implantation and the changes in the time and percent growth of the stented and non-stented vessels (native) were measured (Figure 4.1). The non-stented vessels grew 1.4–3.1 mm per 6 months, whereas the stented vessels always grew at higher rates, ranging from 1.7

to 6.7 mm per 6 months. The stents significantly grew in diameter at an average rate of 49% at 180 days (vs. 23% for the non-stented vessels) and 34% at 90 days (vs. 20% for the non-stented vessels). The smallest vessel stented was the iliac artery which grew by 131%. Overlapping Stents# 1&2 grew by 69% and overlapping Stents# 3&4 grew by 89%. As shown in Table 4.1, the smaller the vessel at the initial implantation the more the percentage of growth independent of stent COF or design.

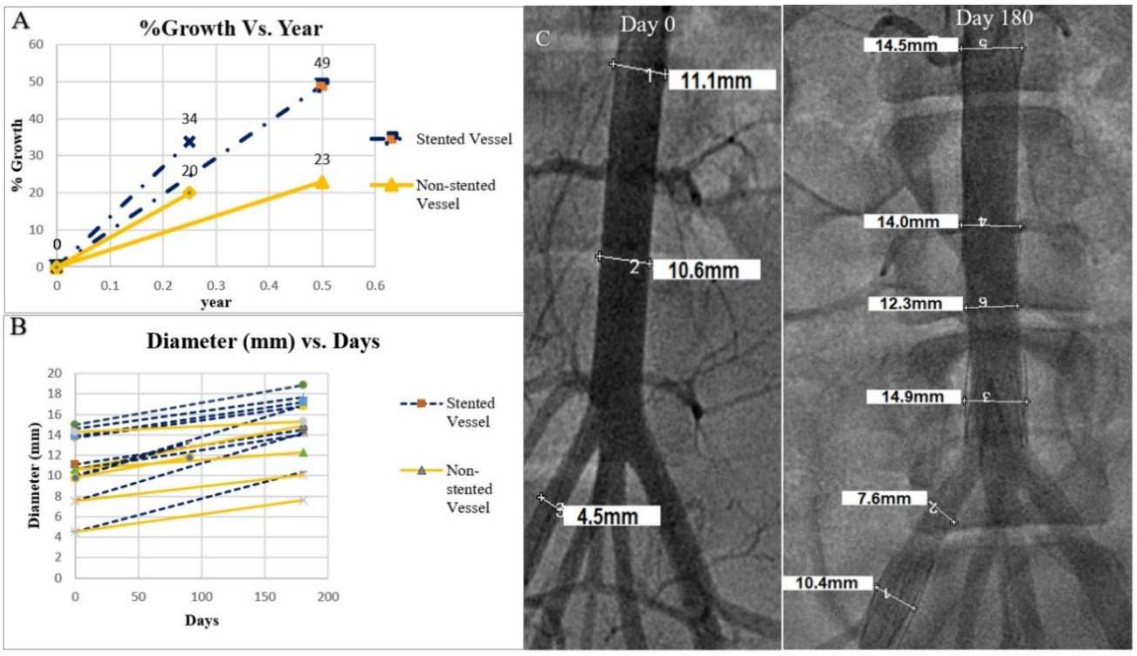

Figure 4.1: Quantitative angiography and stent growth at 90 and 180 days.(A) Percent growth versus year for the native and stented vessels. (B) The absolute growth of stented and non-stented vessels versus days. (C) The angiographic representation of the abdominal aorta and iliac artery at 0 and 180 days after implantation with quantitative analysis.

4.2 Histopathology Summary

Morphometric & histologic comparison of cross-sectional vessel is summarized in Table 2 for all stents. Mean injury score ranges from 0.70 to 1.23 and inflammatory scores ranged from 2.3 to 3.0 at 90 days but decreased uniformly to less than 1.4 by 180 days. Low levels of granuloma

were observed at 90 days which resolved by the 180 days. Low number of giant cells was observed in all animals and the amount of stenosis was less than 11% for all stents except Stent# 4 in animal B which was 20%. Stent# 1 and 2 were implanted for 90 days in the abdominal aorta in Animal A. Radiographic examinations showed that both devices were well deployed at appropriate locations without any stent fractures. Stent# 1 had quantitatively less EEL, IEL, and medial areas and had a smaller luminal area than Stent# 2. Histological findings were comparable in both stents except for giant cells, which were frequently observed in Stent# 2 compared with Stent# 1. Endothelialization was completed in both stents and, while the mean injury score was mild in both stents the neointimal inflammation scores were mild to moderate, granulomas were rarely observed, and adventitial inflammation was minimal. No malposition, uncovered struts, and residual peri-strut fibrin were noted in any of the stents. There was no significant stenoses, aneurysms or dissections in any of the samples.

Stent# 1-4 were implanted for 180 days in the abdominal aorta proximal to distal. In Animal C, Stent# 1&2 along with Stent# 3&4 overlapped. Radiographic examinations showed all implanted stents were well deployed and expanded without any stent fractures. Histological findings were comparable in all three animals and among stents, with the overall mild injury score being slightly higher in Stent# 1. All stents showed a mature layer of neointimal coverage, with large lumen area. Focal mild inflammation was observed in all stents, mostly chronic, without extension to the underlying arterial wall. Adventitial inflammation was observed in one single strut and single section (Animal D, Stent# 3), limited to less than 25% of the stent circumference. The frequency of giant cells was low in all stents, although slightly higher in Stents# 2 and Stent# 3. Endothelialization was completed in all stents, and the neointimal inflammation scores were low. Granulomas were rarely detected in Stent 1 (1.67±2.36) and were absent in Stents# 2, 3, 4 and the

overlapping stents. Malposition was absent in all stents except for Stents 1 and 4 in animal C due to the test artifact. All stents had minimal residual peri-strut fibrin except the overlapping stents.

The health of the media of each artery was specifically evaluated with Trichrome staining. There was variable degree of medial compression and injury in the setting of, a mature neointimal layer around the stent struts were seen in each stent (Figure 4.2). The IEL was lacerated in most samples (Figure 4.2A) except for Stents# 1, 2, and 4 in Animal D. The EEL in all samples was intact and did not exhibit any signs of tear or laceration (Figure 4.2C). The media was intact in most samples except for Stent# 2 in Animal A and Stent# 4 in Animal B (stent in the iliac artery in which the stent had eroded all the way through the media (Figure 4.2D).

Despite the injury pattern, especially with the struts perforating through the media and toward the adventitia, the neointimal response was minimal and uniform for up to 90 and 180 days. All the histopathology results are summarized in Table 4.2 through Table 4.4

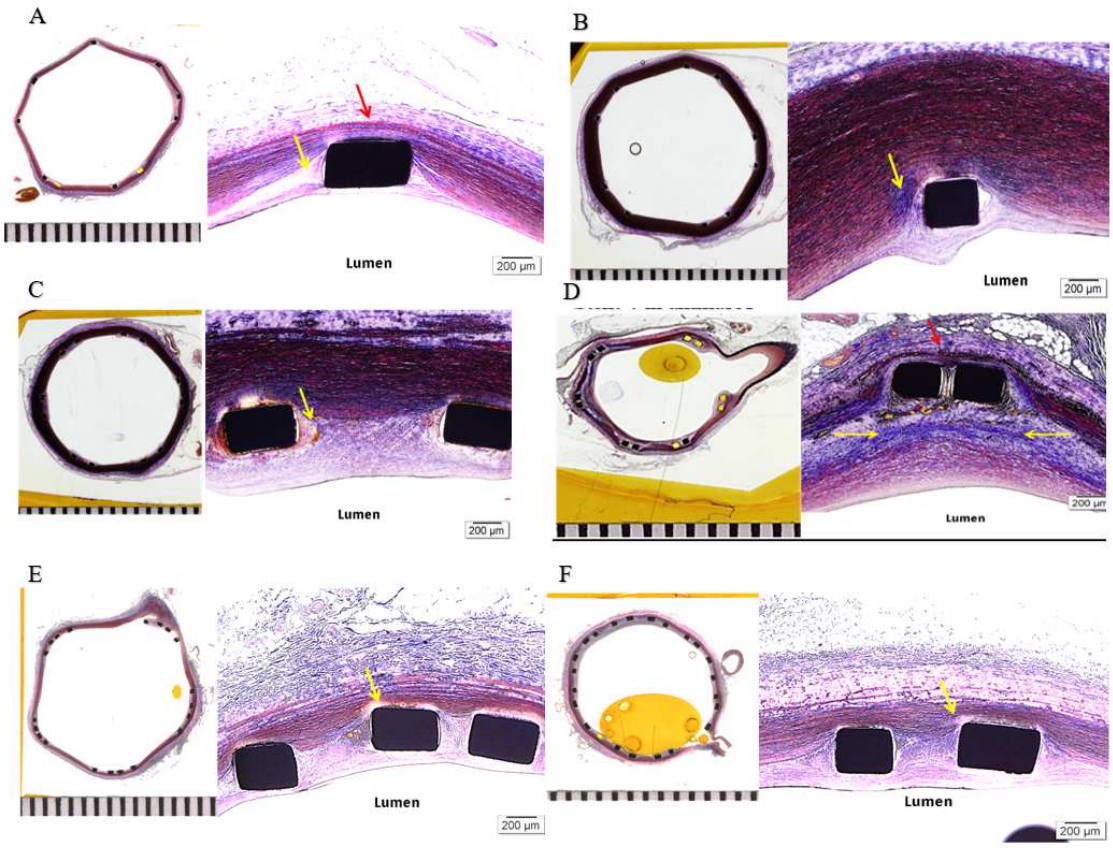

Figure 4.2: Representative histopathological cross-sectional images. (A) Stent# 1, (B) Stent# 2, (C) Stent# 3, (D) Stent# 4, (E) overlapping Stents# 1&2, and (F) overlapping Stents# 3&4. Black squares represent stent struts. Yellow arrows indicate focal collagen deposition around struts, whereas red arrows indicate medial compression.

There was not a direct correlation between the amount of COF at the time of implantation and the amount of stents growth nor was a strong correlation between degree of histopathology results and COF. Stent# 4 in Animal B with the least amount of COF grew the highest and caused the most injury and stenosis (Figure 5D) versus Stent# 1 with higher COF did not grew as much and did not cause a significant injury (Figure 5A).

4.3 Angiography and Histology

In this section the detail findings regarding the quantitative angiography and histopathology after placing the designed stents into the abdominal aorta of rapid growing porcine arteries are presented.

4.3.1 Quantitative Angiography

Figure 4.3, represent the quantitative angiography of animal's abdominal aorta prior to the implantation (0 day) and after duration of the designed study (90 or 180 days). Figure 4.3A represent section of the abdominal aorta for Animal A, 90 days study with two stents implanted in this animal. Figure 4.3B represent the section of the abdominal aorta along with the iliac with stents for Animal B. Three stents implanted proximal to distal in the abdominal aorta and one stent implanted accidentally in the iliac artery. Figure 4.3C represents section of the abdominal aorta for Animal C. Four stents were implanted in the abdominal aorta of Animal C, Stent# 2 was implanted inside the Stent# 1 and the Stent# 4 implanted inside the Stent# 3. Figure 4.3D represents section of the abdominal aorta for Anima D. All other stents were appropriately implanted in this animal. Angiography for each animal was performed as it was explained in the method section with measurements.

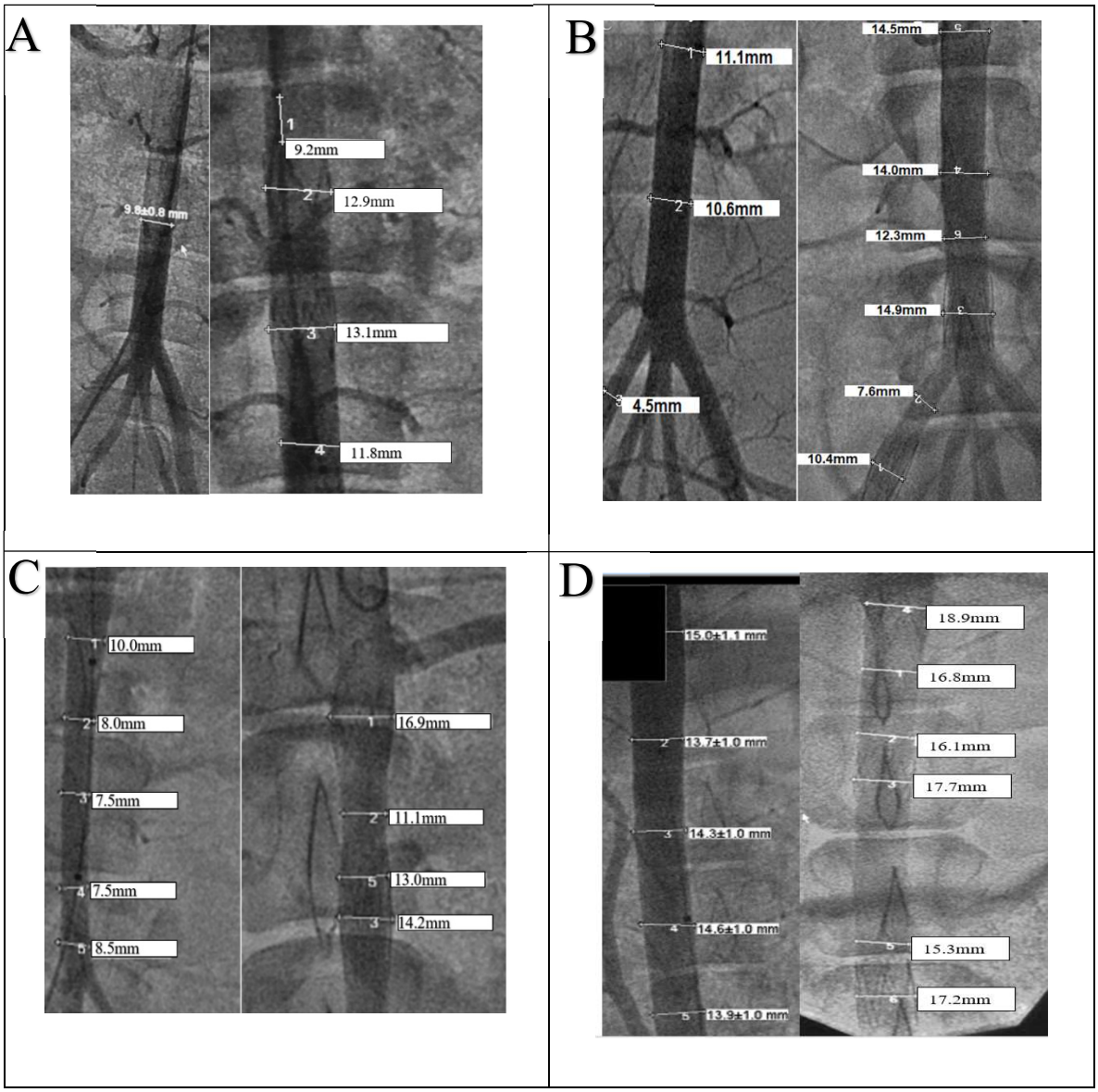

Figure 4.3: Quantitative angiography images of all four animals. (A) Represents Animal A with a duration of 90 days with only two stents in the abdominal aorta. (B) Represents Animal B with three stents in the abdominal aorta and one stent inside the iliac. (C) represent Animal C with overlapping Stent# 1&2 and Stent# 3&4. (D) represents Animal D with 4 stents in the abdominal aorta. All stents were implanted in appropriate location with no issues. Contrast shot was used during the angiography to show the patency of the vessel's lumen. Quantitative analysis performed for each stents' growth and reported.

4.3.2 Radial Force Analysis

Representative fabricated self-expanding stents were tested in the radial force tester as explained in the method section and the hysteresis for each stent was generated (Figure 3.3). The angiographic images were analyzed, and the vessel diameter was measured for each stent prior to the implantation and after the duration of the study as explained in the method section. From the radial force study and the hysteresis results it was possible to find the amount of force exerted on the vessel at the time of implantation as reported in Table 4.1. The growth measurements and the stent chronic outward forces at the time of implantation was plotted in Figure 4.4. A strong correlation between the vessel growth and the stent force was not identified, rather a correlation between the location of the stent and growth and injury was observed. The low force stents in the distal side of the artery grew more than the high force stents in the proximal side.

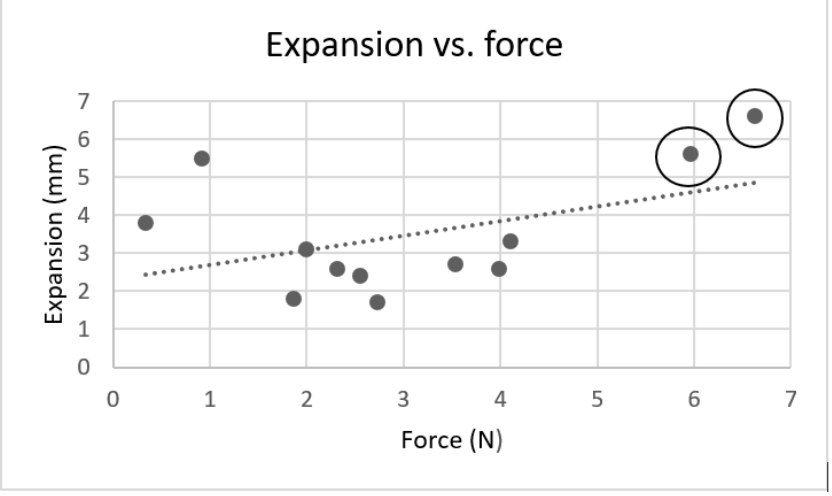

Figure 4.4: Expansion of vessel diameter vs. force of stents. It was observed the low force stents in the distal side of the artery grew higher than the high force stents in the proximal side. Two data points shown with circles are overlap Stent# 1&3 and Stents# 3&4. There was not a strong correlation between force and the expansion of the vessel.

4.3.3 Histopathology

In Animal A, two stents implanted in the abdominal aorta for 90 days. In Animal B, three stents implanted in the abdominal aorta, and one stent in the iliac artery. In Animal C, Stent# 2 implanted inside the Stent# 1 and Stent# 4 implanted inside the Stent# 3 (stent in stent). In Animal D, four stents implanted in the abdominal aorta for a duration of 180 days.

The stented segments are submitted for plastic processing with H&E staining. The non-stented segments proximal and distal to the stents are submitted for paraffin processing with H&E staining. Middle section of each stent was submitted for Elastic Trichrome staining.

Orthogonal radiographic was performed for each stented segment and the position and expansion of each stent was evaluated. Figure 4.5 shows the radiographic image. Stent 1 is marked with lines to show the proximal, middle, and distal section of the stent. All the stents are well opposed and widely expanded without any intraluminal thrombus.

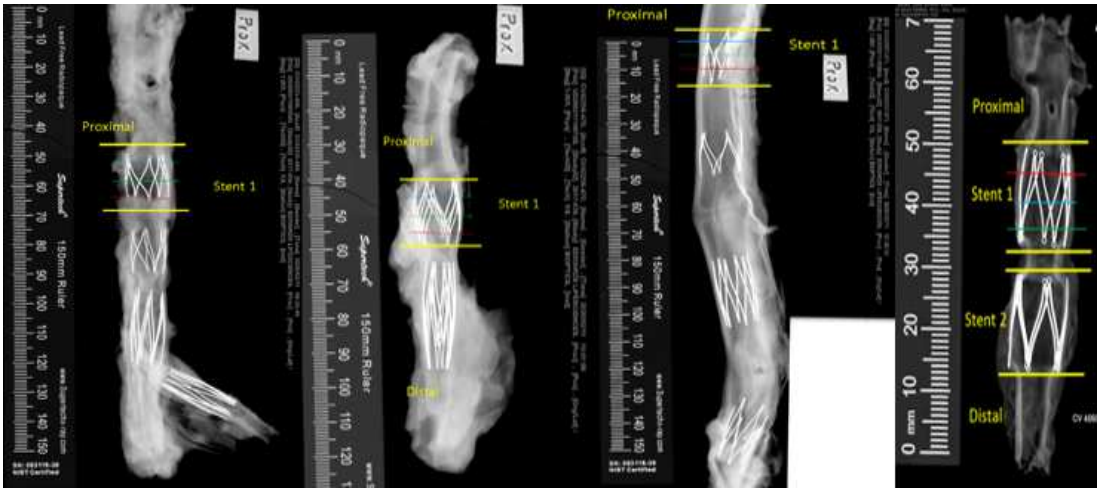

Figure 4.5 Orthogonal radiographic images. Representative image of orthogonal radiographic of all the stents. Lines show the proximal, middle, and distal side of Stent# 1. all the stents are well opposed and widely expanded without any intraluminal thrombus.

Paraffin histology of the non-stented segments of the aortas (proximal and distal to the stented regions, the yellow line in for all stents (Figure 4.5) with H&E staining for all animals and

Movat staining for Animal A, showed minimal changes in the arterial lumen. the distortion of the lumen is a test artifact. For Animal A, proximal marked as A and B and inter-stent segments as C and distal marked as E and F. For Animal B, proximal to distal, marked as A1.1, A2.1 and A3.1. In the proximal and distal sections of iliac stent (Stent# 4) the H&E staining showed focal intimal thickening in the proximal section (B1.1) while minimal changes are observed in the distal post-stented section (B2.1). For Animal C, proximal to distal marked as, A1.1, A2.1 and A3.1. for Animal D proximal marked as A.1.1, A.3.1, A.5.1, and A7.1, and distal marked as A2.1, A4.1, A.6.1 and A8.1.

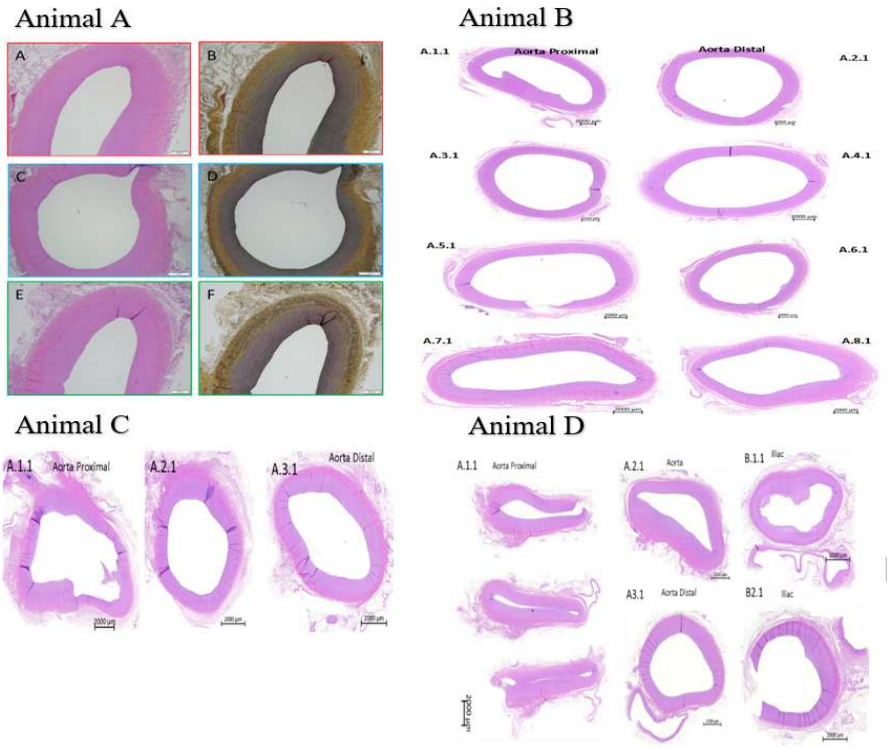

Figure 4.6: Non-stented segments of aorta paraphing histology Distortion of the lumen is a test artifact. Minimal changes noticed in the non-stented sections**.** For Animal A, proximal marked as A and B and inter-stent segments as C and distal marked as E and F. With H&E and Movat staining. For Animal B, proximal to distal, marked as A1.1, A2.1 and A3.1. In the proximal and distal sections of iliac stent (Stent#t 4) the H&E staining showed focal intimal thickening in the proximal section (B1.1) while minimal changes are observed in the distal post-stented section (B2.1). For animal C, proximal to distal marked as, A1.1, A2.1 and A3.1. for Animal D proximal marked as A.1.1, A.3.1, A.5.1, and A7.1, and distal marked as A2.1, A4.1, A.6.1 and A8.1

4.3.3.1 Stent# 1 processed with plastic histopathology and H&E staining

Stent# 1 has an average chronic outward force of 5N. This stent implanted in the proximal side of the abdominal aorta. Figure 4.7 represent the plastic processed stented segment of the aorta with H&E staining. The following is the summary of the findings for Stent 1 in Animal A, B, C and D.

Stent# 1 in Animal A. In Figure 4.7 Image A shows a proximal histological image, B is the middle power image and C is the high-power image, which shows thinning media due to compression by struts and some inflammatory cells consisting of macrophages and lymphocytes, as well as thick mature neointimal coverage with surface endothelialization. Image D corresponds to the middle section; E and F are high power images of D corresponding to each color of boxes; calcification and inflammatory cells surrounding struts are seen in image F; Image G is the distal section in the Stent# 1, while H and I are the high-power images from G, showing focal minimal granulomatous reaction around single struts (H); minute foreign material is shown in image I.

Stent# 1 in Animal B. In Figure 4.7, the upper row shows a histological image of the most proximal aspect of the stent (A), B is the middle power image showing peri strut chronic inflammation (red box) and C is a high-power image, which shows thinning media (yellow arrows) due to compression by struts and some inflammatory cells consisting of macrophages and lymphocytes. Image D corresponds to the middle section, while E is a high-power image showing thick mature neointimal coverage with surface reendothelialization. Image F is the distal section in the Stent# 1, while G and H are high power images of F corresponding to mature neointimal coverage with surface endothelialization and chronic inflammation around strut (blue box).

Stent# 1 in Animal C. Stent# 2 implanted in Stent# 1. In Figure 4.7 (A) the image above the upper row shows a histological image of the most proximal aspect of the Stent# 2 in Stent# 1.

B is the middle power image from A, which shows thinning media due to compression by struts and neovessel formation with few extravasated red blood cells (yellow box). Image C corresponds to the mid-section; image D is the high-power from C showing focal peri strut calcification. Image E correspond to the distal section; F shows areas of peri strut calcification and mild chronic inflammation (blue arrows) (Stained with H&E).

Stent# 1 in Animal D. In Figure 4.7 A shows the most proximal aspect of Stent# 1, B is the middle power image which shows peri strut chronic inflammation (yellow box) and thick mature neointimal coverage with surface endothelialization. Image C correspond to the middle section; D is high power images of C showing focal peri strut residual fibrin and scattered inflammatory cells. Image E correspond to the distal section of the stent; F is high power images of E showing focal peri strut chronic inflammatory cells in between struts consisting of macrophages and lymphocytes

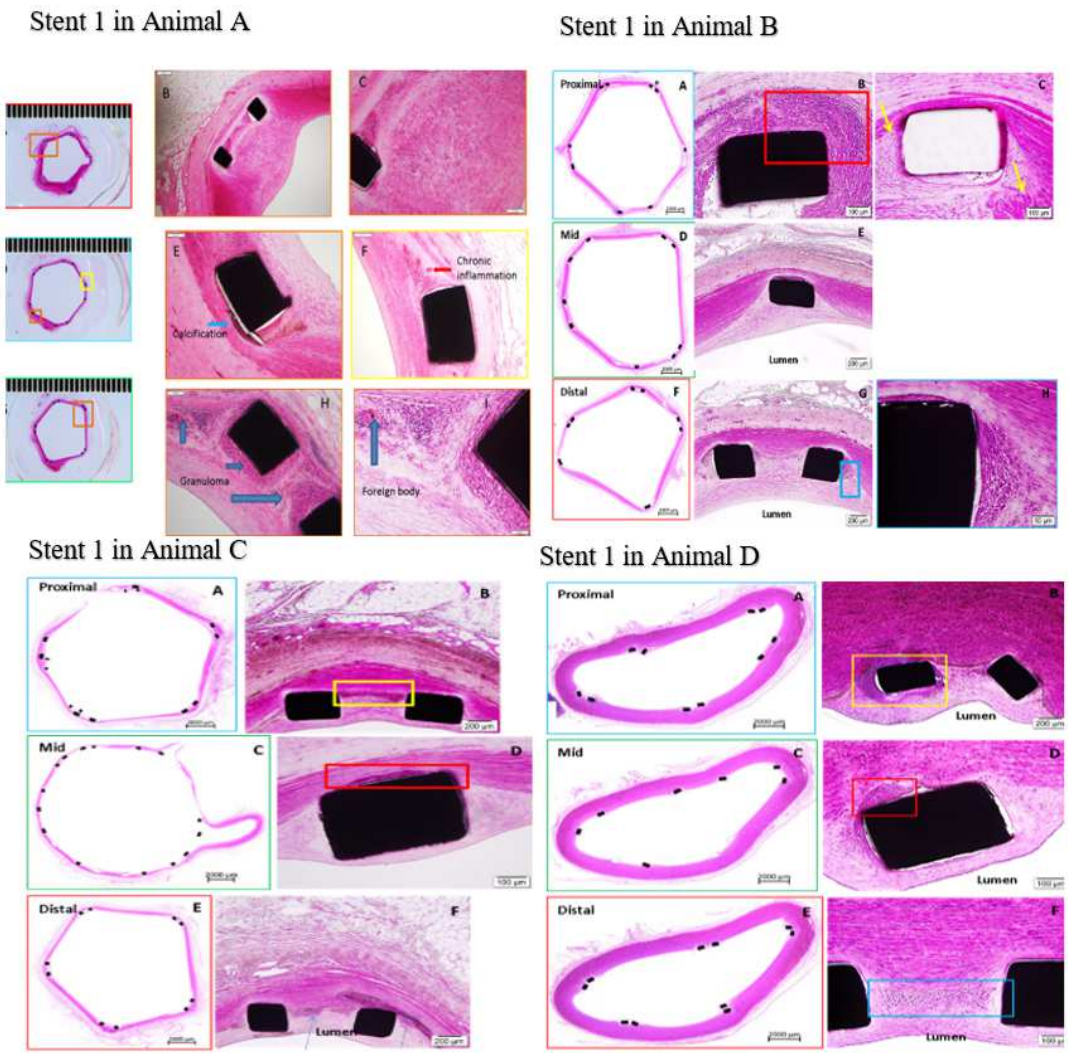

Figure 4.7: Histological images from Stent 1 in Animal A, B, C and D (H&E staining). Stent# 1 is a stent with an average chronic outward force of 5N. This stent implanted in the proximal side of the abdominal aorta. Animal C had a overlap Stent# 1&2.

4.3.3.2 Stent# 1 processed with plastic histopathology and Elastic Trichrome staining

Plastic histopathology with Elastin Trichrome staining in Figure 4.8 showed all the struts well opposed to the aortic wall and covered by neointimal tissue. The middle power images showing compression of the medial layer by stent strut without laceration, (red arrow and yellow box). Focal collagen deposition around the struts of the stent observed (yellow arrows) as shown in the image. IEL lacerated in animal B and C and stayed intact in Animal A and D. EEL compressed but intact in all animals.

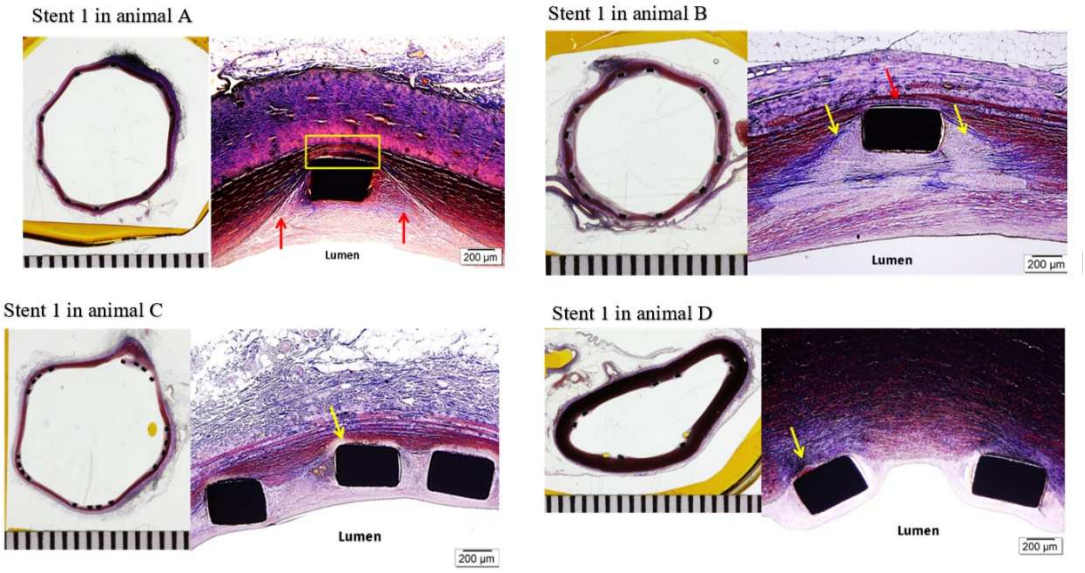

Figure 4.8: Histological images from the Stent# 1 with Elastin Trichrome staining. compression of the media observed in all samples (red arrow and yellow box). No laceration of the medial layer in any of the stents. IEL lacerated in Animal B and C. IEL stayed intact in Animal a and D. EEL compressed but intact in all samples. focal collagen deposition around struts was observed (yellow arrows).

4.3.3.3 Stent# 2 processed with plastic histopathology and H&E staining

Stent# 2 in Animal A. In Figure 4.9, images labelled B, C, and D are the high-power images corresponding to the colored boxes in image A (left column). Following observations noticed in Stent# 2 in Animal A: Image B: peri-strut calcification; Image C: medial compression; Image D: inflammatory cells surrounding a strut. Image F: calcification and giant cells around a single strut; Image G: chronic inflammatory infiltrate around single strut; Image H is the distal section in the Stent# 2 and I and J are the high-power images from H, showing calcification around struts (I) and inflammatory cells including giant cells (J).

Stent# 2 in Animal B. in Figure 4.9 the upper row shows a histological image of the most proximal aspect of the stent (A); B is the middle power image, which shows thinning media due to compression by struts and thick mature neointimal coverage with surface endothelialization (red arrow). Image C corresponds to the middle section; D is the high-power image of C corresponding to an area with peri strut inflammation (yellow boxes). Image E is the distal section in Stent# 2 while F is the high-power image from E, showing focal peri strut calcification (blue arrow) with mature neointimal coverage and endothelialization of the strut and minimal inflammation.

Stent# 2 in Animal D. In Figure 4.9**,** the upper row shows a histological image of the most proximal aspect of the stent (A), B is the high power of A, which shows moderate focal chronic inflammation cells consisting of macrophages and lymphocytes (blue box). Image C corresponds to the middle section; D is a high power of C showing focal moderate peri strut chronic inflammation. Image E is the distal section in the Stent# 2, while F is the high-power image from E, showing focal mild granulomatous reaction around single strut (yellow box) and mature neointima covering the struts.

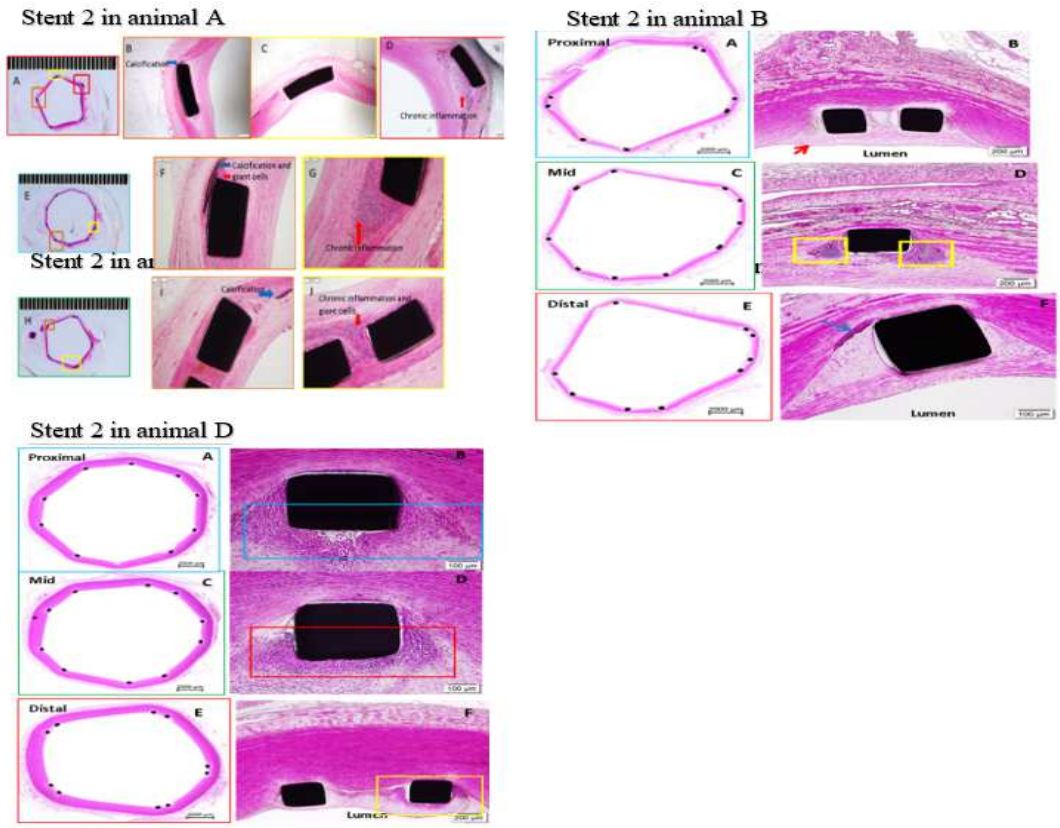

Figure 4.9: Histological images from Stent# 2 in Animal A, C and D (H&E staining). Stent# 2 has an average chronic outward force of 2.5N. This stent implanted in the proximal side of the abdominal aorta after Stent# 1. In Animal C the Stent# 1&2 overlapped therefore the data are not shown here.

4.3.3.4 Stent# 2 processed with plastic histopathology and Elastic Trichrome staining

Plastic histopathology with Elastin Trichrome staining in Figure 4.10 showed all the struts well opposed to the aortic wall and covered by neointimal tissue. The middle power image shows compression of the medial layer by the stent strut without laceration (red arrow) in Animal A and B. in Animal A compression of the medial layer (yellow box) by stent strut with focal laceration is shown. Focal collagen deposition around struts (yellow arrows) was observed. IEL lacerated in Animal A and B. IEL is intact in Animal D but compressed. EEL is compressed and intact in all animals.

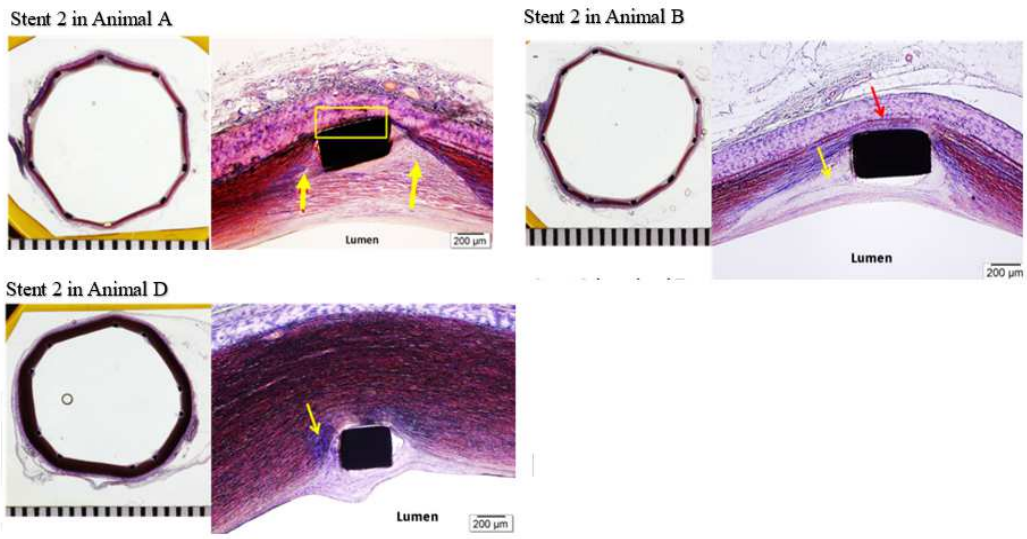

Figure 4.10: Histological images from Stent# 2 with elastin Trichrome staining. compression of the media (red arrow and yellow box) observed in all the samples with focal laceration of the media in Stent# 2 in Animal D. IEL lacerated in Animal A and D and intact in Animal C. EEL compressed but intact in all samples. Focal collagen deposition around struts was observed (yellow arrows).

4.3.3.5 Stent# 3 processed with plastic histopathology and H&E staining

Stent# 3 has an average chronic outward force of 3N. This stent implanted in the more distal side of the abdominal aorta. Figure 4.11 represent the plastic processed stented segment of the aorta with H&E staining. The following is the summary of the findings for Stent# 3 in Animal B, C, and D:

Stent# 3 in Animal B. in Figure 4.11**,** the upper row shows a histological image of the most proximal aspect of the stent (A); B is the middle power image and C is the high-power image, which show thinning media due to compression by struts and some inflammatory cells consisting of macrophages and lymphocytes (red box) and thick mature neointimal coverage with surface endothelialization. Image D corresponds to the middle section, while E is a high-power image of D showing chronic inflammation around a strut (yellow boxes). Image F is the distal section in the Stent# 3, while G is the high-power image from F, showing focal chronic inflammation around single struts.

Stent# 3 in Animal C. Stent# 4 implanted in Stent 3. In Figure 4.11, the image above the upper row shows a histological image of the most proximal aspect of the stent (A); B is the middle power image**;** and C is the high power image of the proximal section, which show thinning of the media due to compression by struts; some inflammatory cells are also observed consisting of macrophages and lymphocytes and thick mature neointimal coverage with surface endothelialization; hemosiderin deposits are also observed (blue box). Image D correspond to area of calcification and bone formation around single strut. Image E is the low power of the distal aspect of the stent; F shows focal disruption of the media and thick mature neointima covering the strut.

Stent# 3 in Animal D. In Figure 4.11 the image above, the upper row shows a histological image of the most proximal aspect of the stent (A); B is the middle-power image, which show thinning media due to compression by struts and thick mature neointimal coverage with surface endothelialization of strut (blue arrow). Image C corresponds to the middle section, while section D is the high-power image of C showing focal moderate adventitial chronic inflammation mostly lymphocytic (red box). Image E is the distal aspect of the stent, with F showing a high power of a strut from E with focal residual peri strut fibrin and minimal inflammatory cells.

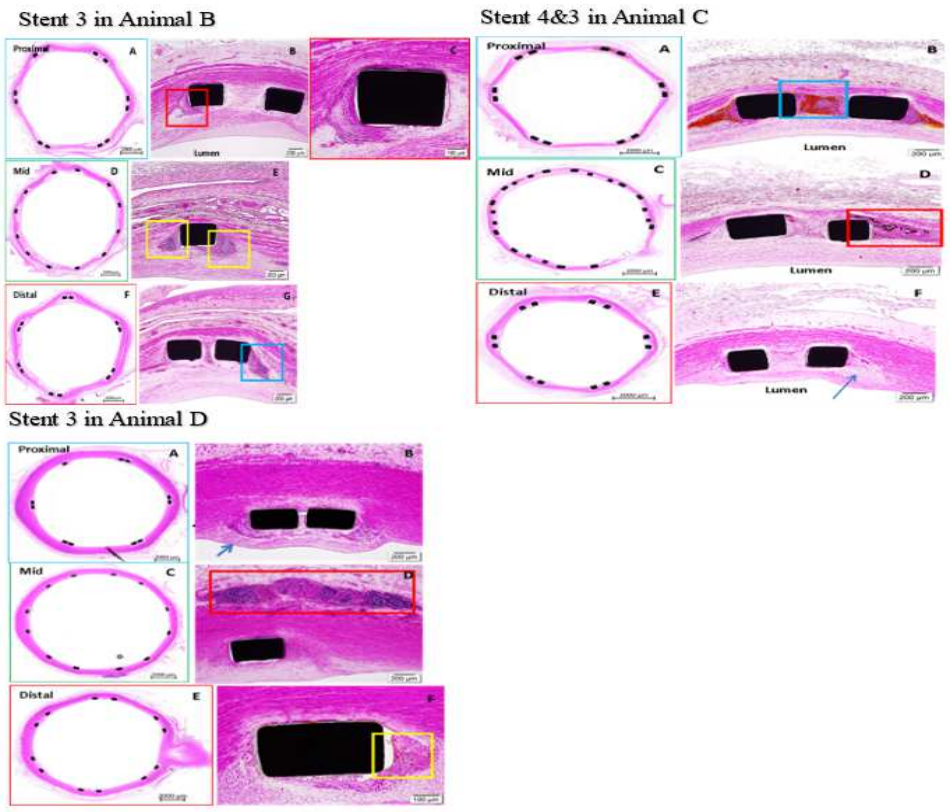

Figure 4.11: Histological images from Stent# 3 in Animal A, B, and C (H&E staining). Stent# 3 with an average chronic outward force of 3.0N. This stent implanted in more distal side of the abdominal aorta after Stent# 2. Stent# 3 was not implanted in Animal D.

4.3.3.6 Stent 3 processed with plastic histopathology and Elastic Trichrome staining

Plastic histopathology with Elastin Trichrome staining in Figure 4.12 showed all the struts well opposed to the aortic wall and covered by neointimal tissue. The middle power image shows compression of the medial layer by the stent strut without laceration (red arrow) in any of the samples. Focal collagen deposition around struts (yellow arrows) was observed. IEL lacerated in all animals. EEL is compressed and intact in all animals.

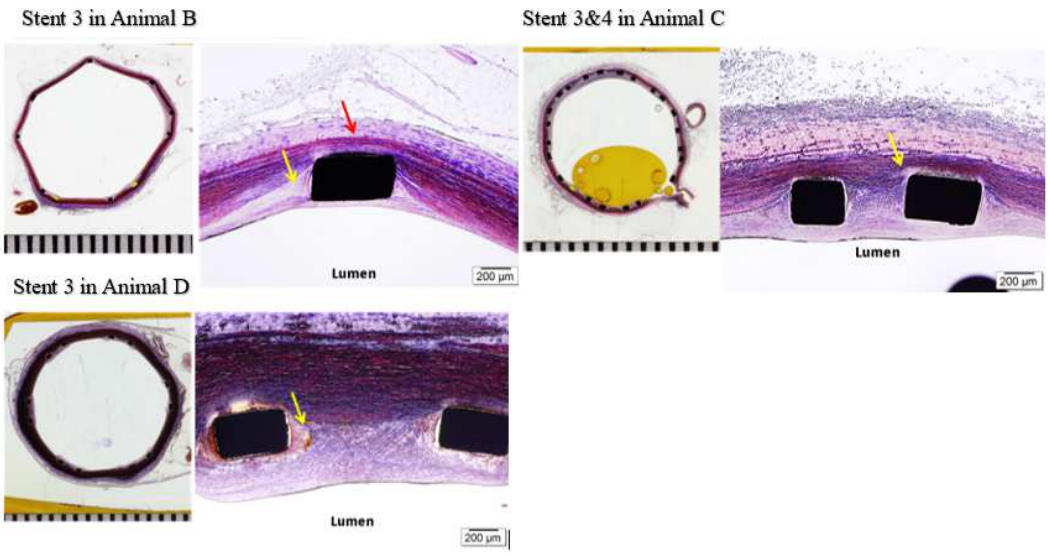

Figure 4.12: Histological images from Stent# 3 with elastin Trichrome staining compression of the media (red arrow) observed in all the samples with no laceration of the media in any of the samples. IEL lacerated in all animals. EEL compressed but intact in all samples. Focal collagen deposition around struts was observed (yellow arrows).

4.3.3.7 Stent# 4 processed with plastic histopathology and H&E staining

Stent# 4 has an average chronic outward force of 0.5N. This stent implanted in the distal side of the abdominal aorta/iliac. Figure 4.13 represents the plastic processed stented segment of the aorta with H&E staining. The following is the summary of the findings for Stent# 4 in Animal B, and D. There is no data for Animal B since Stent# 4 implanted in Stent# 3 in this animal:

*Stent# 4 in Animal B***.** In Figure 4.13 Figure 4.11, the upper row shows a histological image of the most proximal aspect of the stent (A); B is the middle power image, which shows thinning and laceration of the media (blue box) due to compression by struts and some inflammatory cells consisting of macrophages and lymphocytes (red boxes) and thick mature neointimal coverage with surface endothelialization. Image C corresponds to the middle section; D is the high-power image of C corresponding to an area with peri strut inflammation (red boxes). Image E corresponds to the distal section; and F is a high-power image of E corresponding to an area of peri strut inflammation.

Stent# 4 in Animal D. In Figure 4.13 the upper row shows a histological image of the most proximal aspect of the stent (A); B is the high-power image of A, which shows peri strut fibrin deposits in between struts (red box); Image C corresponds to the middle section of the stent; D is a high-power image showing peri strut residual fibrin and hemosiderin deposits. Image E is the distal section in the Stent# 4, while F is the high-power images from E, showing mature neointima covering the struts, with focal extravasation of red blood cells.

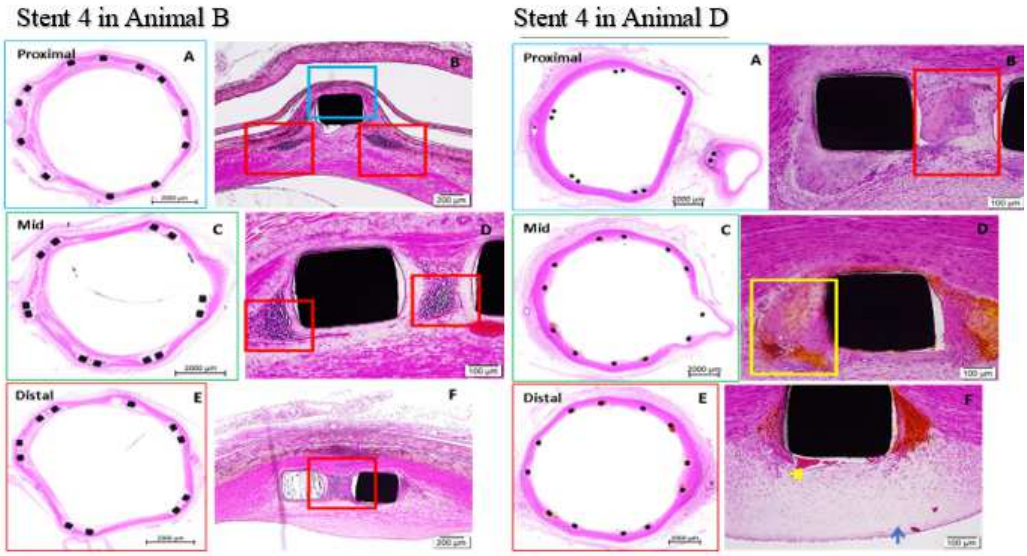

Figure 4.13: Histological images from Stent# 4 in Animal A and C (H&E staining). Stent 4 has an average chronic outward force of 0.5N. This stent implanted in the distal side of the abdominal aorta/iliac after Stent# 3. Stent# 4 was implanted in Stent# 3 in Animal B and Stent# 4 was not implanted in Animal A.

4.3.3.6 Stent# 4 processed with plastic histopathology and Elastic Trichrome staining

Plastic histopathology with Elastin Trichrome staining, Stent# 4 was implanted in the iliac in animal B. Figure 4.14 shows all the struts well opposed to the aortic wall and covered by neointimal tissue. The middle power image shows compression of the medial layer by the stent strut with laceration (red arrow) in Animal B. Focal collagen deposition around struts (yellow arrows) was observed. IEL lacerated in Animal A. IEL is intact in Animal D. EEL is compressed and intact in all animals.

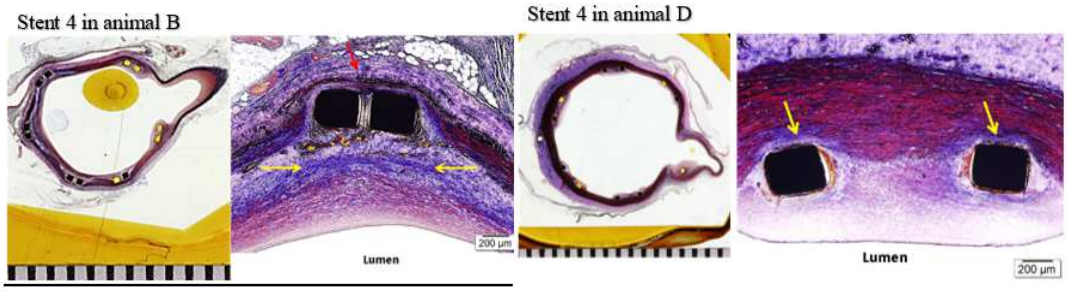

Figure 4.14: Histological images from Stent# 4 with elastin Trichrome staining compression of the media (red arrow) observed in all the samples with laceration of the media in Animal B. the stent implanted in iliac of Animal B. IEL lacerated in all animals. EEL compressed but intact in all samples. Focal collagen deposition around struts was observed (yellow arrows).

4.4 Quantitative Histomorphometric Analysis Summary

In this section the quantitative histomorphometric analysis per section 3.6.3 is summarized

Table 4.2: Morphometric comparison of cross-sectional vessel areas and neointimal thickness

Stent	No. of vessels	EEL Area (mm^2)	IEL Area (mm^2)	Lumen Area (mm^2)	Medial Area (mm^2)	Neointimal Area (mm^2)	Stenosis (%)	Medial Thickness (mm)	Neointimal Thickness (mm)
180 Days duration									
Stent# 1	n=2	138.95±17.45	112.25±0.43	105.29±1.17	30.61±23.41	6.77±1.87	6.02±1.62	0.77±0.58	0.18±0.04
Stent# 2	n=2	132.51±38.52	105.97±19.70	100.22±19.72	26.54±18.82	5.75±0.02	5.52±1.05	0.69±0.45	0.15±0.03
Stent #1 & 2 overlapped	n=1	122.43	111.90	105.10	10.52	6.80	6.10	0.27	0.10
Stent# 3	n=2	113.17±24.38	90.71±14.31	81.52±16.27	22.46±10.07	9.19±1.96	10.40±3.77	0.66±0.21	0.29±0.12
Stent# 4	n=2	71.79±41.97	59.15±30.54	51.80±31.45	12.63±11.43	7.35±0.91	14.68±9.12	0.48±0.32	0.27±0.09
Stent# 3 & 4 overlapped	n=1	65.55	58.39	50.73	7.16	7.66	12.79	0.32	0.14
90 Days duration									
Stent# 1	(n=1, 3 sections)	85.47±12.17	74.63±14.44	68.02±16.63	10.83±2.55	6.61±2.31	9.54±5.43	0.36±0.11	0.36±0.34
Sten#t 2	(n=1, 3 sections)	107.72±12.83	96.41±13.57	89.52±12.1	11.31±1.92	6.89±1.58	7.10±0.79	0.35±0.10	0.28±0.12

Table 4.3: Histologic comparison of cross-sectional vessel

Stent	No of vessels	Mean Injury Score	Neointimal Inflammation Score	Mean Fibrin Score	Fibrin %	Calcification (%)	Granuloma (%)	Giant cell (%)
			180 Days duration					
Stent# 1	n=2	1.16±0.79	1.17±1.18	0.17±0.24	16.67±0.00	8.33±11.79	1.67±2.36	8.33±11.79
Stent #2	n=2	0.71±0.82	0.83±0.71	0.00±0.00	8.33±2.36	7.08±10.02	0.00±0.00	11.67±11.79
Stent# 1 & 2 overlapped	n=1	0.87	0.67	0.00	0.00	6.67	0.00	0.00
Stent# 3	n=2	0.70±0.56	0.50±0.71	0.50±0.71	16.67±23.57	3.33±4.71	0.00±0.00	11.39±11.39
Stent# 4	n=2	0.90±1.01	1.33±0.94	0.83±0.71	27.78±3.93	10.56±14.93	0.00±0.00	8.61±0.39
Stent# 3 & 4 overlapped	n=1	1.13	0.33	0.00	0.00	5.56	0.00	16.67
			90 Days duration					
Stent# 1	n=1 (3 sections)	1.13±0.06	2.33±1.53	0.00±0.00	0.00±0.00	6.67±11.55	6.67±11.55	6.67±11.55
Stent# 2	n=1 (3 sections)	1.23±0.21	3.00±0.00	0.00±0.00	0.00±0.00	23.33±15.28	3.33±5.77	40.00±10.00

Table 4.4: Histologic comparison of cross-sectional vessel

Stent	No of vessels	Malapposition (%)	RBC (%)	Endothel (%)	Uncovered struts (%)	Adventitial inflammation score
			180 Days duration			
Stent# 1	n=2	1.39±1.96	3.33±4.71	100.00±0.00	0.00±0.00	0.17±0.24
Stent# 2	n=2	0.00±0.00	1.67±2.36	100.00±0.00	0.00±0.00	0.17±0.24
Stent# 1 & 2 overlapped	n=1	0.00	3.33	100.00	0.00	0.00
Stent# 3	n=2	0.00±0.00	4.17±5.89	100.00±0.00	0.00±0.00	0.17±0.24
Stent# 4	n=2	3.33±4.71	19.44±7.86	100.00±0.00	11.39±16.11	0.00±0.00
Stent# 3 & 4 overlapped	n=1	0.00	0.00	100.00	1.39	0.00
			90 Days duration			
Stent# 1	(n=1, 3 sections)	0.00±0.00	23.33±5.77	100.00±0.00	0.00±0.00	0.33±0.58
Stent# 2	(n= 1, 3 sections)	0.00±0.00	20.00±10.00	100.00±0.00	0.00±0.00	0.67±0.58

4.5 Summary of Chapter 4

In this chapter the findings after quantitative angiography and histopathology analysis was reported. The summarized data showed the novel self-expanding stent grew with the arteries without inhibiting arterial growth. Also, it was reported stents caused injury to the arterial wall by lacerating the IEL and the media in some of the stented arterial segments. The stent is growing over time and is moving toward the adventitia in some of the samples. It was observed the stents in the distal side (smaller arteries) grew more than the stents in the proximal. The neointima formed around the struts and in the lumen of the artery, however all the lumens stayed patent with no intraluminal thrombus, stenosis, or obstruction. The summary of the morphometric comparison of cross-sectional vessel areas and the histologic comparison of cross-sectional vessels was reported in this chapter.

CHAPTER 5: DISCUSSION

Stenting has emerged as a generally superior option as compared to balloon angioplasty and surgical repair for CoA in infants and children.[14] Nevertheless, the exponential growth of the arteries in children limits the use of stents and requires serial stent redialation and sometimes even fracture or surgical removal.[2] Thus, among pediatric interventional cardiologists, there is a high level of interest in stents that can resorb or grow with the artery. Such stents could eliminate or reduce future reinterventions.[56] This study represents the first effort to evaluate the effects of a purpose-built self-expanding stents on rapidly growing vessels. A range of novel self-expanding nitinol stents were specifically designed and manufactured and used to examine the effects of radial force and stents geometry on the biology of rapidly growing arteries.

5.1 Growth

By varying the geometry and thickness of the nitinol in the stents, four stents with a variety of radial forces were designed, manufactured and tested. The outward force of each stent was measured at each diameter (Table 4.1) and used to correlate the effects of radial force on biology. These custom-made novel stents easily and reliably crimped and deployed in all the animals with good apposition to the aortic wall. None of the stents limited arterial growth and there was continuing stent expansion with time, without erosion of the stents completely through the vessels. On average stented vessels grew 14% and 26% more in diameter at 90 and 180 days respectively than the distal and proximal non-stented segments of the vessels, suggesting that the force against the stented artery segments was higher than needed in all cases. The small vessels (≤10mm) grew to larger degrees as compared to larger vessels (>10mm). The experience with these stents suggests that even lower radial force stents may be ideal for this application. There was a favorable neointimal response and no aneurysm was noted in any of the stented vessels. Thus, angiographic

results of each implantation universally showed that the stents were able to grow with and beyond the native arteries.

5.2 Histopathology

Neointimal ingrowth after use of self-expanding stent has been reported to lead to the narrowing or stenosis of the arterial lumen, thus reducing the luminal area.[2,17,] Compression and tension (mechanical forces) by the stent struts, wall injury, and peri-strut inflammation due to responses to a foreign body object (i.e., stent struts) can cause in-stent stenosis as well as a disruption to the arterial wall leading to long term aneurysms and dissections. [1449,57]. All the stents tested in this study formed a mature neointima layer around the stent struts and none had significant luminal stenoses (5%–20%). However, a wide range of damage to the IEL and media was observed: Figure 5.1A shows stent 4 in the iliac artery, with IEL and media laceration. Furthermore, Figure 5.1B shows Stent 4 in the abdominal aorta with compressed but intact IEL and media. The rupture or laceration of the media or IEL is directly associated with stenosis development.[58,59] All stented segments showed patency without any intraluminal thrombus or obstruction, with <20% stenosis in the worst case, despite compression and injuries of the IEL and the medial layer at 90 and 180 days. The long-term effects of the medial lacerations could not be assessed in a six month study. Fortunately, early re-endothelialization was ubiquitous: there was 100% endothelialization of all stents.

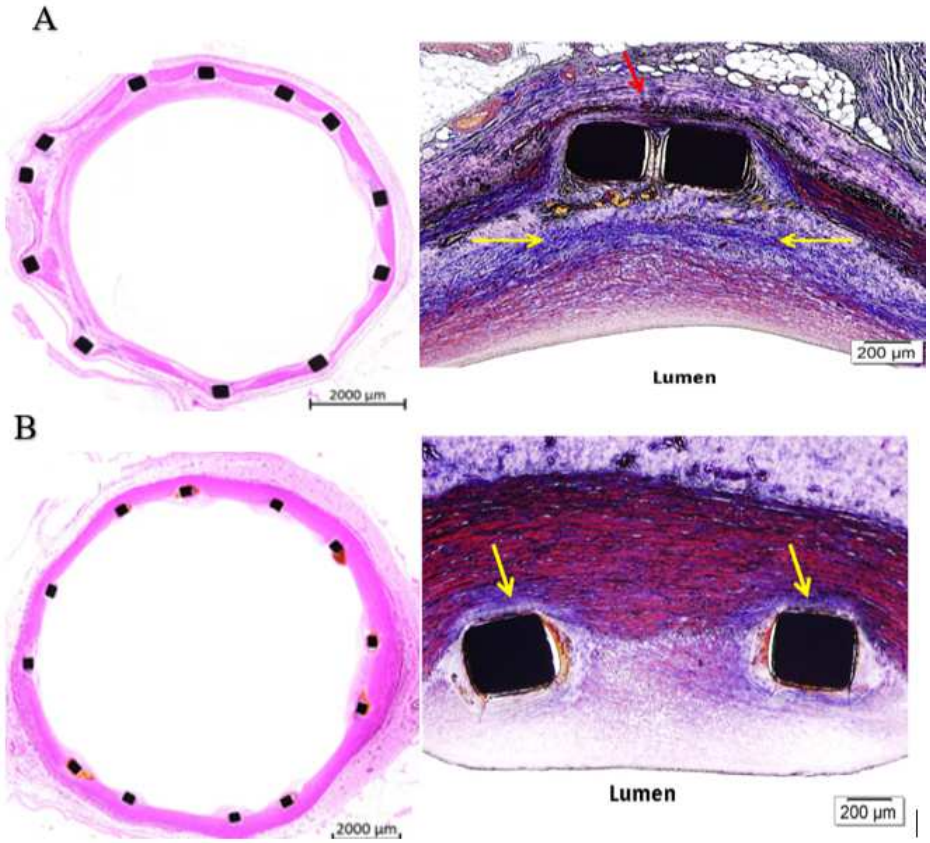

Figure 5.1: Representative histological images from Stent# 4 (A) Shows Stent# 4 in the iliac artery with compression (red arrow) and media and IEL laceration. (B) Stent# 4 in the abdominal aorta with focal aortic medial layer compression by stent strut with compressed but intact IEL and EEL and neointimal layer formation. The image on the left is H&E staining, while that on the right is ET staining. Black squares are stent struts. Focal collagen deposition around the strut is observed (yellow arrows).

The radial force of the stents could not be correlated with the stent's effect on histopathology. No significant correlation was observed between the neointima formation and the forces in the designed stents. Overall injury, and inflammation, value for each stented section were scored according to Schwartz et al.'s scoring scheme (Table 3.3). These criteria have been widely used in stent literatures. High injury scores, particularly scores of 2–3, have been reported to yield thicker neointima formation in the porcine coronary arteries.[22] Because the force on each stented artery was a function of both the stent type as well as the diameter of the stented vessel, an attempt

was made to correlate radial force with vascular injury and histopathology. While the outward force of the stents did not correlate to biological response, it was noted that smaller arteries in general had higher levels of injury and stenosis regardless of stent force. The mean average injury score was comparable among all stents with higher percent stenosis for stents on the distal side of the abdominal aorta.

5.3 Stent Geometry

It is hoped that the data presented in this study will aid in the design of the ideal self-expanding pediatric stent. Clearly, this observations in this limited study support the idea that such a device has the potential to improve outcomes in pediatric stenting. Nonetheless, many parameters need to be optimized in designing a pediatric self-expanding stent. This stent needs to have the ability to deploy via a 4-5 Fr system and then expand to 14-20 mm without overstretching the arterial lumen and causing stenosis, medial laceration or unwanted inflammatory responses. It needs to have enough force to at least growth with the vessel even after neointima formation.[23]
In this study, the stents in smaller vessels had higher mean nominal stent diameter to artery diameter ratios (4.4 vs. 1.4) and higher degrees on medial injury. However, the long-term consequences of this medial injury remain unknown and it can be mitigated using lower radial force stents. Each vessel in the body has different properties therefore when a stent is being designed, the geometry, structure, and mechanics of the target vessel should be considered.

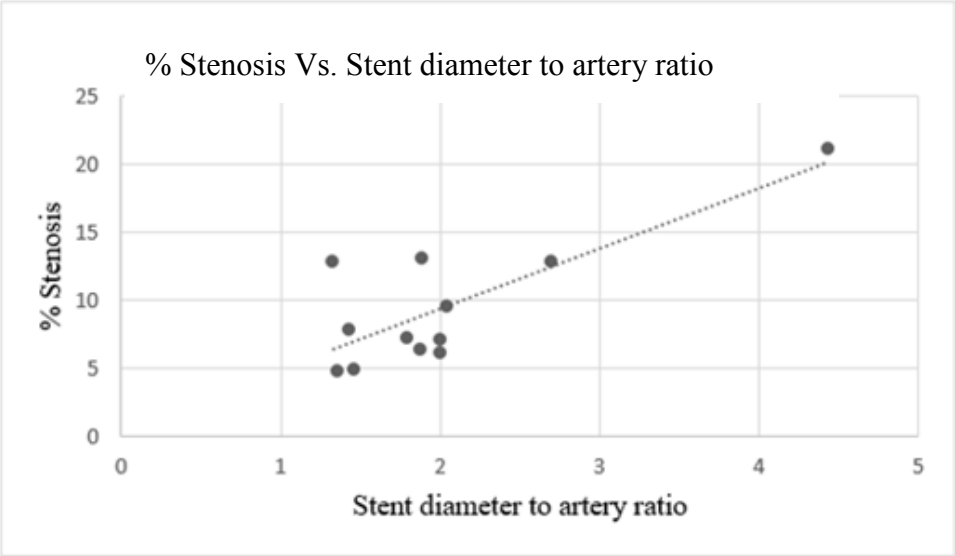

Figure 5.2: Percent stenosis vs. stent diameter to artery ratio Nominal stent diameter for all stent was 20mm. Stents were crimped and implanted into the arteries and over expanded the artery by the ratio between 1.4 to 4.4. Graph demonstrated that percent stenosis increases as the stent diameter to artery ration increases.

Each stent's length was also a key element in restenosis after percutaneous coronary interventions; the longer stents especially in smaller arteries had more stenosis. Additionally, the large number of strut apices is associated with the reduction in neointimal thickening due to more circular arteriographic contour and turbulent flow reduction. [24] When a stent is deployed inside an arterial lumen it will stretches the vessel, imposing a cross-sectional polygonal luminal shape that depends on the stent design, with each strut serving as an apex. [60] In this study Stent# 1 and 2 have five strut apices and Stent# 3 and 4 have six strut apices. The arteriographic counter for the middle of Stent# 2 and Stent# 3 is shown in the image below:

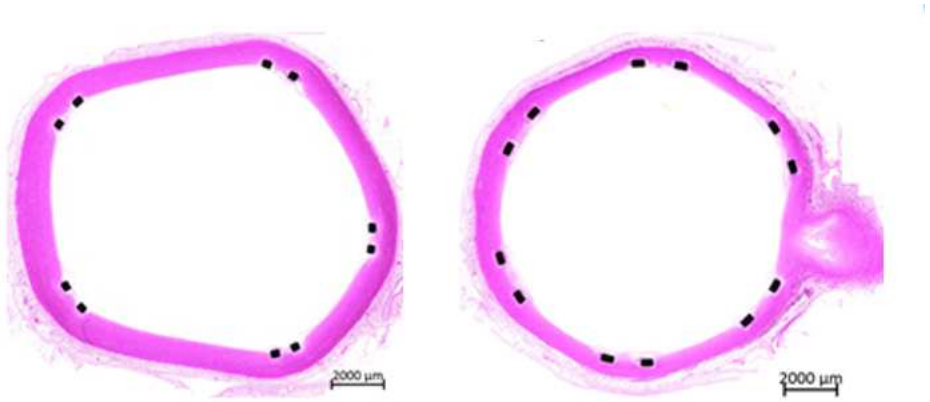

Figure 5.3: Arterial lumen arteriographic contour. Image on the left shows the arterial lumen contour of a vessel with 5 strut vertices (Stent #2) and image on the right shows the arterial lumen counter of a vessel with 6 strut vertices (Stent #3). lumen on the right is more circular than lumen on the left with less struts.

Several groups have examined the fluid dynamics governing blood flow through stented arteries. [61,62,63] These studies concluded circular shape of the vessel lumen will optimize fluid flow characteristics at the blood/tissue interface, reducing regions of turbulence and/or stagnation in the immediate vicinity of stent struts. Laminar flow within the lumen of more circular stented arteries may decrease the platelet and inflammatory cell adhesion and activation, therefore, reducing neointimal hyperplasia [60]. Although there was not a significant difference of stenosis between stents with five apices versus stents with six apices but Garasic et al., argued altering lumen shape by increasing the number of struts per cross section from 8 to 12 was associated with a 50% to 60% drop in mural thrombus burden after 3 days and a 2-fold reduction in neointimal thickening after 28 days in rabbit arteries [60]. Therefore, more strut numbers and regularity of strut distribution provides a more circular vascular lumen which is associated with a smoother, more homogeneous arteriographic contour and more beneficial for the performance of a stent and needs to be considered for the future novel stent designs.

5.4 Study limitation and Conclusion

Although this study was the first study to examine the effects of self-expanding stents on growth vessels, it was not enough for the assessment of complete aneurysm formation and full stent expansion in the arteries. Longer studies are needed to assess for late aneurysm formation or erosion as well as stenosis. While this data set shows growth, it is not able to determine the extent of the stented vessel expansion. Will these stents ultimately expand to their full potential? If not, how close will they get. Future studies should consider more animals, longer implant times and should examine lower-radial force stents as well as various stent geometries and stent placement in different vessels.

Stents that can grow with a small but rapidly growing artery can be designed and could be ideal for several pediatric applications. Despite obvious medial injury in some cases, all stents in this study grew with and beyond the native vessel's growth without development of stenoses, aneurysms or dissections. Although this data set only includes 3- and 6-month pathology, it is likely to be useful in the design of the ideal set of pediatric growth stents.

REFERENCES

[1] Rao PS. Stents in the management of heart disease in children. *Pediat therapeut*. 2013; 3; 2:1-4.

[2] Peters B, Ewert P, Berger F. The role of stents in the treatment of congenital heart disease: Current status and future perspectives. *Ann Pediatr Cardiol*. 2009; 2:3-23.

[3] Linde DVD, Konings EEM, Slager MA, Witsenburg M, Helbing WA, Takkenberg JJM, Ross-Hsselink JW. Birth prevalence of congenital heart disease worldwide: a systematic review and meta-analysis. *J Am Coll Cardio.* 2011;15; 58:2242-2247.

[4] Bernier PL, Stefanescu A, Samoukovic G, Tchervenkov CI, The challenge of congenital heart disease worldwide: Epidemiologic and demographic facts. *Semin. Thorac. Cardiovasc. Surg*. 2010;13: 26–34.

[5] Gilboa SM, Devine OJ, Kucik JE, Oster ME, Riehle-Colarusso T, Nembhard NW, Xu P, Correa A, Jenkins K, Marelli AJ, Congenital heart defects in the United States: Estimating the magnitude of the affected population in 2010. *Circulation*. 2016;134: 101–109.

[6] Doshi AR, Chikkabyrappa S. Coarctation of Aorta in Children. *Cureus*. 2018; 10: e3690.

[7] Bjornard K, Riehle-Colarusso T, Gilboa SM, Correa A. Patterns in the prevalence of congenital heart defects, metropolitan Atlanta, 1978 to 2005. *Birth Defects Res Part A Clin Mol Teratol*. 2013; 97:87-94.

[8] Moore K, Persaud TVN, Torchia M. Saunders. The Developing Human: Clinically Oriented Embryology. 2016; 11th edition.

[9] Russell GA, Berry PJ, Watterson K, Dhasmana JP, Wisheart JD. Patterns of ductal tissue in coarctation of the aorta in the first three months of life. *J Thorac Cardiovasc surgery.* 1991; 102:596-60.

[10] Rudolph AM, Heymann MA, Spitznas U. Hemodynamic considerations in the development of narrowing of the aorta. *Am J Cardiol*. 1972; 30:514–525.

[11] Suradi H, Hijazi ZM. Current management of coarctation of the aorta. *Glob Cardiol Sci Pract*. 2015; 2015:44-55.

[12] Kank JS. Treatment of restenosis of coarctation by percutaneous transluminal angioplasty *Circulation*. 1983; 68:1087-1094.

[13] Morrow WR, Smith VC, Ehler WJ, van Dellen AF, Mullins CE. Balloon angioplasty with stent implantation in experimental coarctation of the aorta. *Circulation*. 1994; 89:2677-2683.

[14] Forbes TJ, Kim DW, Du W, Turner DR, Holzer R, Amin Z, Hijazi Z, Ghasemi A, Rome JJ. Comparison of surgery, stent and balloon angioplasty treatment of native coarctation. An observational study by the CCISC (congenital Cardiovascular Interventional Study consortium). *J Am Coll Cardiol 2011;* 58: 2664-2674.

[15] Haji-Zeinali A, Ghasemi M. Coarctoplasty with self-expandable stent implantation for treatment of coarctation of aorta in adults. *Arch. Iranian Med*. 2006; 9:348-353.

[16] Morgan G J, Pushaparajah K, Narayan S, Rosenthal E. Large calibre self-expanding Stents for pulmonary stenosis after the arterial switch, a low-risk solution to a low-flow situation. *Pediatr Cardiol*. 2018; 39:824-828.

[17] Cheung YF, Sanatani S, Leung M, Human D, Chau KT, Culham JAG. Early and intermediate-term complications of self-expanding stents limit its potential application in children with congenital heart disease. *J Am Coll Cardiol.* 2000; 35:1007-1015.

[18] Siegenthaler M, Celik R, Haberstroh J, Bajona P, Goebel H, Brehm K, Euringer W, Beyersdorf. Thoracic endovascular stent grafting inhibits aortic growth: An experimental study. *Eur J Cardiothorac Surg*. 2008; 34:17-24.

[19] Bedoya J, Clark A, Meyer LH, Timmins MR, Moreno JE, Moore. Effects of stent design parameters on normal artery wall mechanics. *J Biomech Eng*. 2006;128: 757-765.

[20] Schmidt T, Abbott JD, Coronary Stents: History, Design, and construction. *J Clin Med*; 2018 7: 126.

[21] Beule MD. Biomechanical Modeling of Stents: Survey 1997-2007. Advances in Biomedical Engineering. 2009; 61-93.

[22] Stoeckel, Pelton, Duerig, Self-Expanding Nitinol Stents: Material and design considerations. *Eur Radiol*. 2004;14(2):292-301.

[23] ShabaJovskaya S. On the nature of the biocompatibility and medical applications of NiTi shape memory and superelastic alloys. *BioMed Mat Eng*. 1996; 6:267-89.

[24] Duerig TW, Pelton AR, Stöckel D. The use of superelasticity in medicine. *Metall*. 1996; 50:569-574.

[25] Fortier A, Gullapalli V, Mirshams RA. Review of biomechanical studies of arteries and their effect on stent performance, *IJC Heart Vessels* 2004;4:12-18.

[26] Majesky MW, Rong Dong X, Hoglund V, Mahoney WM, Daum G. The adventitia A dynamic interface containing resident progenitor cells. *Arterioscler Thromb Vasc Biol*. 2011; 31:1530-1539.

[27] Sommer G. *Mechanical properties of healthy and diseased human arteries*. [dissertation]. Austria: Verlag der Technischen Universitat Gax; 2010.

[28] Han HC, Fung YC. Longitudinal strain of canine and porcine aortas. *J Biomech.* 1995;28(5):637-641.

[29] Hong X, Gu W. Plasticity of vascular resident mesenchymal stromal cells during vascular remodeling. *Vascular Biology*. 2019;1:H67-H73.

[30] Shakti AG, Guo L-W, Liu B, Kent KC. Mechanisms of post-intervention arterial remodeling, *Cardiovasc Res*. 2012;96:363-371.

[31] Hill MA. Embryology HM practical - Blood vessel histology. (2020, July 25) Retrieved from https://embryology.med.unsw.edu.au/embryology/index.php/HM_Practical_-_Blood_Vessel_Histology.

[32] Bondanza S, Calevo MG and Marasini M. Early and Long-Term results of Stent Implantation for Aortic Coarctation in Pediatric Patients Compared to Adolescents: A Single Center Experience. *Cario Res Pract*. 2016;2016: 4818307.

[33] Long AL, Page PE, Raynaud AC, et al. Percutaneous iliac artery stent: Angiographic long-term follow-up. *Radiology* 1991; 180:771-778.

[34] Rousseau HP, Raillat CR, Joffre FG, et al. Treatment of femoropop-liteal stenoses by means of self-expandable endoprostheses: Midtermresults. *Radiology* 1989; 172:961-964.

[35] O'Laughlin MP, Slack MC, Grifka RG, et al. Implantation and intermediate-term follow-up of stents in congenital heart disease. *Circulation* 1993; 88:605–14.

[36] Ing FF, Grifka RG, Nihill MR, Mullins CE. Repeat dilation of intravascular stents in congenital heart defects. *Circulation* 1995; 92:893-937.

[37] Shaffer KM, Mullins CE, Grifka RG, et al. Intravascular stents incongenital heart disease: Short- and long-term results from a large single-center experience. *J Am Coll Cardiol* 1998; 31:661-667.

[38] Hong MK, Beyar R, Kornowski R, et al. Acute and chronic effects of self-expanding nitinol stents in porcine coronary arteries. *Coron Artery Dis*. 1997; 8:45-48.

[39] Freeman JW, Snowhill PB, Nosher JL. A link between stent radial forces and vascular wall remodeling: The discovery of an optimal stent radial force for minimal vessel restenosis. *Connect Tissue Res*. 2010; 51:314-26.

[40] Timmins LH, Miller MW, Clubb Jrand FJ, Moore JE. Increased artery wall stress post-stenting leads to greater intimal thickening. *Lab Investig*. 2011; 91:955-967.

[41] Fontaine AB, Spigos DG, Eaton G, et al. Stent induced intimal hyperplasia: Are there fundamental differences between flexible and rigid stent designs*? J Vasc Interv Radiol.*1994;5:739-744.

[42] Zhao HQ, Nikanorov A, Virmani R, Jones R, Pacheco E, Schwartz LB. Late stent expansion and neointimal proliferation of oversized Nitinol stents in peripheral arteries. *Cardiovasc Intervent Radiol*. 2009; 32:720-726.

[43] Saguner AM, Traupe T, Räber, et al. Oversizing and restenosis with self-expanding stents in iliofemoral arteries. *Cardiovasc Intervent Radiol*. 2012; 35:906-913.

[44] Barth KH, Virmani R, Froelich J, Takeda T, Lossed SV, Newsome J, Jones R, Lindisch D. Paired comparison of vascular wall reactions to Palmaz stents, Strecker tantalum stents, and Wallstents in canine iliac and femoral arteries. *Circulation*. 1996; 93:2161-2169.

[45] Lossef SV, Lutz RJ, Mundorf J, Barth KH. Comparison of mechanical deformation properties of metallic stents with use of stress-strain analysis. *J Vasc Interv Radiol*.1994; 5:341-349.

[46] Flueckiger F, Sternthal H, Klein GE, Aschauer M, Szolar D, Kleinhappl G. Strength, elasticity and plasticity of expandable metal stents: in vitro studies with three types of stress. *Vasc Interv Radiol*.1994;5:745-750.

[47] Sakaoka A, Souba J, Rousselle SD, et al. Different vascular responses to a bare nitinol stent in porcine femoral and femoropopliteal arteries. *Toxicol Pathol.* 2019;47: 408-417.

[48] Haji Zeinali AM, Sadeghian M, Qureshi SA, Ghazi P. Midterm to long-term safety and efficacy of self expandable Nitinol stent implantation for coarctation of aorta in adults. *Catheter Cardiovasc Interv.* 2017; 90:425-431.

[49] Bugeja J, Cutajar D, Zahra C, Parascandalo R, Grech V, and DeGiovanni JV. Aortic stenting for neonatal coarctation of the aorta - when should this be considered? *Images Paediatr Cardiol.* 2016; 18:1-4.

[50] D'Souza S, Ferrante G, Tyczynski P, Mario CD. Biodegradable Stents - A New Era? *European Cardiology*. 2008; 4:82-84.

[51] Sullivan TM, Ainsworth SD, Langap EM, Taylor S, Synder B, Cull David, Youkey J, Laberge M. Effect of endovascular stent strut geometry on vascular injury, myointimal hyperplasia, and restenosis. *J Vas Surg*. 2002; 36:143-149

[52] Bennett, MR, In-stent stenosis: Pathology and implications for the development of drug eluting stents. *Heart*. 2003; 89: 218-224

[53] Timmins LH, Miller MW, Clubb FJ, Moore JE, increased artery wall stress post-stenting leads to greater intimal thickening. *Lab invest*. 2011; 91:955-967

[54] Kheradvar A, Zareian R, Kawauchi S, Goodwin R, Rugonyi S, Animal models for heart valve research and development. *Drug Discovery models*. 2017; 24:55-62

[55] Schwartz, R. S., Huber, K. C., Murphy, J. G., Edwards, W. D., Camrud, A. R., Vlietstra, R. E., and Holmes, D. R. (1992). Restenosis and the proportional neointimal response to coronary artery injury: Results in a porcine model. *J Am Coll Cardiol* 19, 267–74.

[56] Mohan, UR, Danon S, Levi D, Connolly D, Moore JW, Stent implantation for coarctation of the aorta in children. *J Am Coll Cardiol: Cardiovasc Interv*. 2009;2: 877-83

[57] Farb A, Sangiorgi G, Carter AJ, Walley VM, Edwards WD, Schwartz RS, Virmani R. Pathology of acute and chronic coronary stenting in humans. *Circulation*. 1999; 99:44-52.

[58] Farb A, Weber DK, Kolodgie FD, Burke AP, Virmani R. Morphological predictors of restenosis after coronary stenting in humans. *Circulation*. 2002; 105:2974-2980

[59] Indolfi C, Torella D, Coppola C,Stabile E, Esposito G, Curcio A, Pisani A, Cavuto L, Arcucci O, Cireddu M, Troncone G, Chiariello M. Rat carotid artery dilation by PTCA balloon catheter induces neointima formation in presence of IEL rupture. *Am J Physiol Heart Circ Physiol*. 2002; 283:H760–767.

[60] Garasic JM, Edelman ER, Squire JC, Seifert P, Williams MS and Rogers C. Stent and Artery Geometry Determine Intimal Thickening Independent of Arterial Injury. *Circulation*. 2000; 101:812-818

[61] Aenis M, Stancampio AP, Wakhloo AK, Lieber BB. Modeling of flow in a straight stented and nonstented side wall aneurysm model. *J Biomech Eng.* 1997; 119:206–212.

[62] Lieber BB, Stancampio AP, Wakhloo AK. Alteration of hemodynamics in aneurysm models by stenting. *Ann Biomed Eng*. 1997;25: 460–469.

[63] Peacock J, Hankins S, Jones T, Lutz R. Flow instabilities induced by coronary artery stents. *J Biomech*. 1995; 28:17–26.